Light Scattering and Surface Plasmon Resonance on Prism-Metal-Dielectric Coupler

Beang Sengkhun

A Thesis Submitted in Partial Fulfillment of the Requirements for the Degree of Master of Science in Physics

Prince of Songkla University

2017

Light Scattering and Surface Plasmon Resonance on Prism-Metal-Dielectric Coupler

Beang Sengkhun

A Thesis Submitted in Partial Fulfillment of the Requirements for the Degree of Master of Science in Physics

Prince of Songkla University

2017

Thesis Title	Light Scattering and Surface Plasmon Resonance on Prism-Metal-Dielectric Coupler
Author	Mr. Beang Sengkhun
Major Program	Physics

Major Advisor

.....
(Assoc. Prof. Dr. Teparksorn Pengpan)

Examining Committee :

.....Chairperson
(Asst. Prof. Dr. Chesta Ruttanapun)

.....Committee
(Assoc. Prof. Dr. Teparksorn Pengpan)

.....Committee
(Dr. Chalongrat Daengngam)

The Graduate School, Prince of Songkla University, has approved this thesis as partial fulfillment of the requirements for the Master of Science Degree in Physics.

.....
(Assoc. Prof. Dr. Teerapol Srichana)
Dean of Graduate School

This is to certify that the work here submitted is the result of the candidate's own investigations. Due acknowledgement has been made of any assistance received.

……...Signature
(Assoc. Prof. Dr. Teparksorn Pengpan)
Major Advisor

……...Signature
(Mr. Beang Sengkhun)
Candidate

I hereby certify that this work has not been accepted in substance for any degree, and is not being currently submitted in candidature for any degree.

.....Signature
(Mr. Beang Sengkhun)
Candidate

ชื่อวิทยานิพนธ์ การกระเจิงของแสง และการกำทอนของพลาสมอนผิวบนคู่ควบปริซึม-โลหะ-ไดอิเล็คทริค

ผู้เขียน Beang Sengkhun

สาขาวิชา ฟิสิกส์

ปีการศึกษา 2559

ABSTRACT (THAI)

ความก้าวหน้าความรู้ทางด้านวิทยาศาสตร์เกี่ยวกับพลาสโมนิก (Plasmonic) ได้เสนอความคิดที่เป็นกุญแจสำคัญสำหรับการประยุกต์ใช้เทคโนโลยีระดับนาโนตั้งแต่ไบโอเซนเซอร์จนถึงพลาสโมนิกโซลาเซลล์ สำหรับไบโอเซนเซอร์ พลาสโมนิกช่วยให้การตรวจจับของตัววัดมีความไวสูง ส่วนของพลาสโมนิกโซลาเซลล์ช่วยให้แผ่นโซลาเซลล์แปลงพลังงานแสงอาทิตย์ไปเป็นพลังงานไฟฟ้ามีประสิทธิภาพดียิ่งขึ้นโดยควบคุมการเพิ่มปฏิสัมพันธ์ของแสงในแผ่นโซลาเซลล์ พื้นผิวรับและสะท้อนแสงถูกออกแบบให้มีลักษณะพื้นผิวหยาบเพื่อช่วยดักจับหรือการดูดซับแสง พื้นผิวโซลาเซลล์ได้รับการออกแบบให้เป็นตัวเชื่อมแบบไดอิเล็กทริก-โลหะคู่ควบ ซึ่งคล้ายคลึงกับรูปแบบของกรีซชมัน (Kretschmann) ในการศึกษาครั้งนี้ ผู้ทำวิทยานิพนธ์ใช้ซอฟต์แวร์สำเร็จรูป (COMSOL Multiphysics) ที่ดำเนินการโดยใช้ระเบียบวิธีไฟไนต์เอลิเมนต์ (FEM) เพื่อศึกษาความสัมพันธ์ของมุมตกกระทบและความยาวคลื่นของแสงต่อการสะท้อนกลับ การดูดกลืนและการทะลุผ่าน โดยการตรวจสอบและปรับพารามิเตอร์ทางกายภาพ และหาค่าพารามิเตอร์ที่เหมาะสมสำหรับการเกิดเรโซแนนซ์ (resonance) ของพื้นผิวพลาสมอน (SP) ในการศึกษาส่วนแรกผู้ทำวิทยานิพนธ์ได้ศึกษา SiO_2-Ag-air คู่ควบ เพื่อหาค่าความหนาที่เหมาะสมของชั้นเงิน (Ag) สำหรับพื้นผิวเรียบของแผ่นเงิน (Ag-slab) พบว่า หนา 40 nm และสนามแม่เหล็กไฟฟ้าในโหมด TM ที่ตกกระทบบนพื้นผิวมีความยาวคลื่น 565 nm ทำให้เกิดการสะท้อนแสงต่ำสุดและเข้าใกล้ศูนย์ที่มุมของพื้นผิวพลาสมอนเรโซแนนซ์ (PSR) 46° ส่วนพื้นผิวหยาบชนิดแกรตติง สัมประสิทธิ์การสะท้อนแสงมีการจุ่มลงที่มุมอื่น ๆ นอกจากที่มุมของ PSR ในส่วนที่สองผู้ทำวิทยานิพนธ์ได้ทำการออกแบบโครงสร้างของพลาสโมนิกโซลาเซลล์ และตรวจสอบพารามิเตอร์ต่าง ๆ

ได้แก่ รูปทรงของอนุภาค ขนาด ความหนาและระยะห่างของขอบ ในการศึกษาการควบคู่แสงสำหรับพลาสโมนิกโซลาเซลล์ ผู้ทำวิทยานิพนธ์ออกแบบโครงสร้างเป็นสามรูปแบบ รูปแบบแรก อนุภาค Ag ทรงกลมขนาดนาโนถูกฝังอยู่ที่ผิวด้านบน และส่วนด้านล่างของโครงสร้างโซลาเซลล์มี Ag ผิวราบ รูปแบบที่สอง อนุภาค Ag ทรงกลมถูกฝังอยู่ภายในระหว่างชั้นฟิล์มซิลิกอน (Si) และซิลิกอนไดออกไซด์ (SiO_2) และรูปแบบสุดท้ายมีลักษณะผิวเป็นแกรตติง Ag อยู่ที่ชั้นล่างสุดของโครงสร้างโซลาเซลล์ ผลการจำลองเป็นดังนี้ ในรูปแบบแรกคลื่น TM ที่มีความยาวคลื่น 530 nm ตกกระทบบนพื้นผิวด้านบนมีการจุ่มลงต่ำสุดในการสะท้อนกลับหมดของแสงสอดคล้องกับการดูดกลืนสูงสุดที่มุมการสะท้อนของ SP 36° ที่ระยะห่างระหว่าง Ag 160 nm ในรูปแบบที่สองและรูปแบบที่สาม การจุ่มลงในมุมสะท้อนของ SP เกิดขึ้นที่มุม 74° และ 40° โดยคลื่นที่มีความยาว 650 nm และ 460 nm ตามลำดับ และยังพบอีกว่า ที่ระยะห่างระหว่างทรงกลมและระหว่างแกรตติงนาโนขนาด 150 nm, 160 nm, 170 nm และ 180 nm ไม่มีการเปลี่ยนแปลงมุมของการสะท้อนของ SP.

Thesis Title Light scattering and surface plasmon resonance on Prism-Metal-Dielectric Coupler
Author Mr. Beang Sengkhun
Major Program Physics
Academic Year 2016

ABSTRACT (ENGLISH)

Advances in scientific knowledge of plasmonics offer key ideas for nanotechnology applications from biosensors to plasmonic solar cells. For biosensors there are attempts to improve their sensitivity, and for solar cells both their efficiency in energy conversion capability and harnessing by enhancing light-matter interaction, e.g., by designing antireflection surfaces and surface roughing for trapping or absorbing of light. One of the most common models is designed as a dielectric-metal coupler in similar to the Kretschmann's configuration design. In this study, we used COMSOL Multiphysics software implemented with finite element method (FEM) to study the relation of incident angle of light with respect to wavelength, investigate the physical relevant parameters and find the optimal parameters for occurrence of surface plasmon (SP) resonance. In the first part we studied the SiO_2−Ag−air coupler to find the optimal thickness of the silver layer. For smooth surface of the Ag-slab, we found that its thickness of 40 nm yields the minimum reflection close to zero with the electromagnetic field of wavelength of 565 nm incident at the angle of surface plasmon resonance of 46°. For the rough surface of grating type, there are dips at other angles than at the angle of surface plasmon resonance. For the second part, we designed the structures of plasmonic solar cell to investigate the physical relevant parameters and the effect of particle shape, size and array pitch on the coupling of light for the plasmonic solar cell, which can be integrated within the solar cell in three configurations. For the first configuration, the spherical silver nanoparticles (Ag) are imbedded at the top as well as the Ag film at the bottom of the solar cell. For the second one, the Ag nano-spheres are embedded inside between the silicon (Si) and SiO_2 film. For the last one, the Ag gratings are placed at the bottom face of the

plasmonic solar cell. A TM wave with wavelength of 530 nm is incident on the top surface of the first configuration and it was found that the minimum dip in reflection corresponding to the highest absorption occurs at an angle of SP resonance of 36° for the spacing distance between the Ag nano-spheres of 160 nm. For the second and the third configurations where the Ag spheres embedded inside between the Si and SiO_2 interface and the Ag grating at the back of the solar cell, the dips in reflection resonance angle of SP resonance occurs at an angle of 74° and 40° with incident wavelengths of 650 nm and 460 nm, respectively. It is found that for various spacing distances of either the Ag nano-sphere or the Ag grating of 150nm, 160nm, 170nm and 180nm there is no change in angle of SP resonance.

ACKNOWLEDGEMENTS

I would like to express my sincere thanks to my thesis advisor, Associate Professor Doctor Teparksorn Pengpan for his invaluable help and constant encouragement throughout the course of this research while pursuing my master's degree.

I am most grateful for his teaching and advice, not only the research methodologies but also many other methodologies in life. I would not have achieved this far and this thesis would not have been completed without all the support that I have always received from him.

My thanks go to Graduate School, Prince of Songkla University for the research grant in carry out this study, and thanks to the Department of Physics, Faculty of Science, Prince of Songkla University.

I would like to thanks Her Royal Higness Princess Maha Chakri Sirindhorn, who gave scholarships to Cambodian students, having the opportunity to study at universities in Thailand. For this reason, I had the opportunity coming to study for a master's degree at Prince of Songkla University.

Finally, I most gratefully acknowledge my parents and my friends for all their support throughout the period of this research.

Beang Sengkhun

TABLE OF CONTENTS

LIST OF FIGURES

LIST OF TABLES

CHAPTER 1

INTRODUCTION

1.1 Background and Significance of the Problem

The metal nanostructure has been much attention in widespread research since it contains one of the outstanding features, surface plasmon resonance (SPR). SPR is defined as a physical process that can occurs when the plan-polarized light travels and hit on a thin metal film at a specific angle and exhibits the total internal reflection (TIR). In 1902 it was observed by Wood that there is a pattern of anomalous dark band in the reflected light. Otto also explained the surface plasmon phenomenon in 1968 (Park 2015). The SPR has emerged as powerful optical detection techniques for studying label free bio-molecular interaction in real-time within a variety of the diverse applications such as life science, vapor detection, surface coatings, and environmental safety. The SPR technique is based on the fact that, at certain conditions, surface plasmons on a metallic surface can be excited by electromagnetic wave, thereby transforming energy of the photon into energy of the oscillating surface electron, whose quantized energy form is called surface plasmon (Yushanov *et al*. 2012). However, SPR has not been limited to biological physics, for it has been used extensively in electrical engineering, chemistry, theoretical physics, and experimental optics (Earp 1998). The electron charges oscillating in resonance with the incident electromagnetic field is called surface plasmon. There are two common configuration methods used to create plasmon excitation by light: grating configuration method and attenuated total reflection (ATR) method. For the ATR method there are two configuration techniques such as the Kretschmann configuration, in which a thin metal film is sandwiched between a silicon dioxide (SiO_2) and air, and the Otto configuration technique, an air in gap between the metal and SiO_2. However, in both cases, the surface plasmon propagates along the metal surface.

Surface plasmon (SP) is general concept to describe an electrons oscillation on a conductor surface, typically thin metal film. Under an appropriate condition, the light wave can be coupled to the surface plasmon. The incident wave with a wavevector that is close to the surface plasmon mode will exhibit some coupling degree and observed as the analytic signal (Gürel 2009). In Kretschmann configuration, a metal thin film is covered on the incident side by prism and by a test sample on the other side. When light is dispatched into the prism at a specific angle, it is coupled into the plasmon mode without reflecting of light off the metal film to an optical photodetector.

At a certain angle of incidence that light couples to matter, the electrons that are bound to the atoms are stimulated and coherently vibrate in a form so-called plasmon polaritron, as shown in Figure 1.1 (Park 2015). The plasmon polaritons can propagate between interface of the metal and dielectric. This phenomenon occurs within a narrow shell of metal surface because the light cannot deeply penetrate through the metal film. Specifically, if the coherently vibrating electrons below surface of metal thin film form quantum sphere, it is called localized surface plasmon resonance (LSPR). When the size of sphere due to the electrons bound to the atom nucleus is much smaller than the wavelength, the quasi-static approximation is adopted. In other words, the electric field over the nanosphere can be assumed to be constant and the field inside the nanosphere is homogeneous and is related to the E-field.

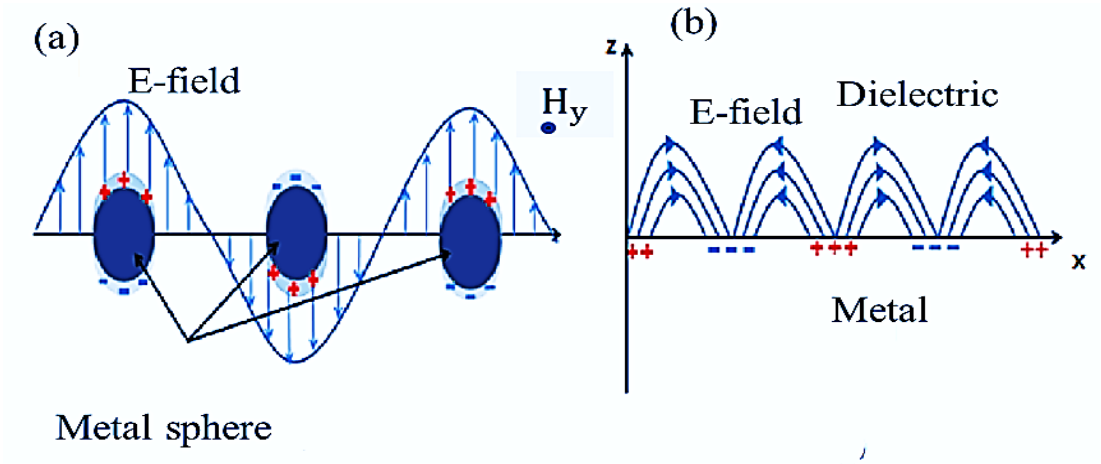

Figure 1.1 Schematic of Surface Plasmon Resonances: (a) localized surface plasmon, the electrons bound to their nucleus at surface of metal film oscillate when the light is shining through and (b) the oscillating charge at the interface between metal surface and dielectric induces EM field.

Under certain conditions, the incident light on a metal surface can couple to this plasmon mode and drive surface plasmons propagating on surface of metal, also known as polarities. Surface plasmon excitation based on TIR when an incident beam of the TM-polarized light hits on an electrically conducting layer at the interface of a medium with high refractive index and an external medium with low refractive index.

Recently, the metal nanostructures supporting surface plasmons have been proposed as an alternative method to achieve light trapping in thin film solar cells (Spinelli *et al*. 2012). Thin film solar cell technology has been developed as a way to reduce the materials costs. Plasmonic solar cell is a type of thin film solar cell which employs plasmon for enhancing light-to-electricity conversion. It improves absorption and scattering of light by using metallic nanostructures that can be excited at its SPR (Müller *et al*. 2004). Incident light at the frequency of plasmon resonance induces surface electrons oscillating at the surface of the metal nano-spheres. The oscillating electrons at the surface of conductor layer can produce an electric current (Catchpole and Polman 2008). One of the common designs is to place metal nano-

spheres on the top of the thin film solar cell surface, as shown in Figure 1.2. When incident light strikes on these metal nano-spheres at their SPR, it will bounce back and forth between the metal nano-spheres and the substrate. In other words, the metal nano-spheres enhance light absorption inside the thin film solar cell layer and, therefore, light-to-electricity conversion.

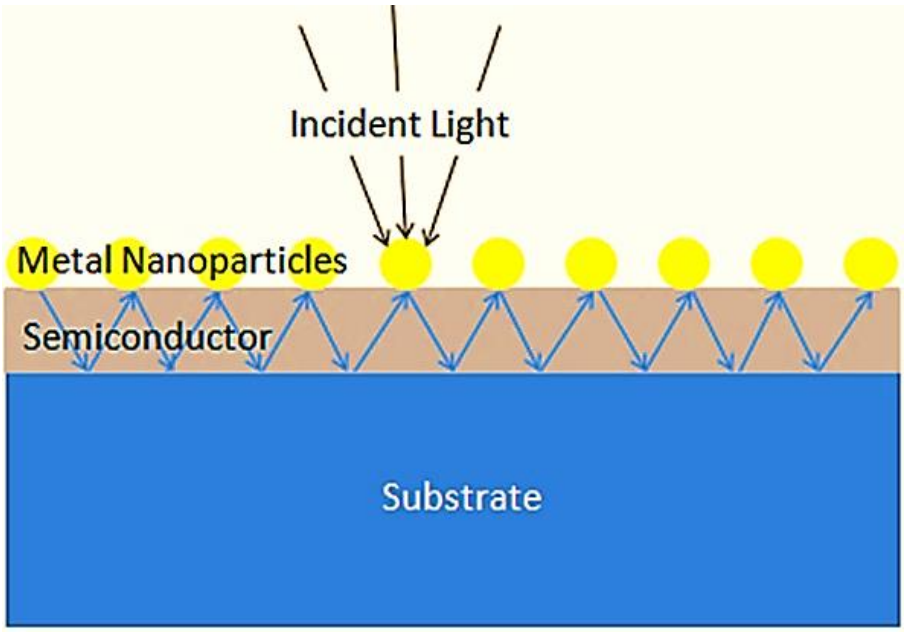

Figure 1.2 Schematic illustration of plasmonic solar cell by using metal nano-spheres placed on the top of the thin film solar cell surface.

1.2 Expected Advantages

1.2.1 Understanding the principle of surface plasmon resonance on SiO_2−Ag−Air Coupler.

1.2.2 Describing the surface plasmon resonance phenomenon and near-field effect on metal nanoparticles within surface metal.

1.2.3 Describing the surface plasmon resonance phenomenon for solar cell.

1.3 Aims of the Research

The light coupling covers the optical properties of the materials, especially layer structures with metal film. The aims of this work are:

1.3.1 To study the relation of incident angle of light with respect to wavelength, investigate the physical relevant parameters in SiO_2−Ag−Air Coupler and find the optimal parameters for occurrence of surface plasmon.

1.3.2 To study surface plasmon resonance and near-field effect due to light scattering on prism-metal-dielectric coupler.

1.3.3 To investigate the physical relevant parameters and the effect of particle shape, size and array pitch on the coupling of light for the plasmonic solar cell.

CHAPTER 2

THEORY AND BACKGROUND

This section introduces the fundamental ideas that are important to comprehend SPR. SPR theory, modulation, techniques, and modeling are discussed. Firstly, we provide theoretical background concerning Maxwell's equations which is fundamental for studying on surface plasmons. Then, we show the wave solutions for surface plasmon rosonance and give conclusions for the necessary conditions to fulfill electron resonance.

2.1 Surface Plasmon Resonance

Surface Plasmon Resonance (SPR) is the resonant oscillation of conduction electrons stimulated by incident light at the interface between a metal film possessing a negative permittivity and dielectric substance with a positive permittivity. The resonance condition is established when the frequency of incident photons matches the natural frequency of surface electrons oscillating against the restoring force of positive nuclei. Scale of nanostructure that can exhibit plasmonic in nature is usually in an order of sub-wavelength of visible light.

The surface plasmon resonance (SPR) depends on interfaces of the metal film with dielectrics, wavelength of the incident light, and the refractive index of both metal film and dielectrics. Because the refractive index is important to perform the measurements at defined temperatures, and also is not dependent on the density of the media (Maier 2007). The metal should have conduction electrons capable of resonating with the incident light at an appropriate wavelength (Shalabney and Abdulhalim 2012). Metals that satisfy this condition are gold, silver, copper, aluminum, indium and sodium. For the metal layer thickness is of great importance in determining the resonance dip in the reflection coefficient profile. The incident light should be monochromatic and p-polarized (polarized in the plane of the surface) to

obtain a resonance dip. All the light that is not p-polarized cannot contribute surface plasmon resonance and will increase the intensity of the reflected light from the metal surface. If the wavelength of incident light is kept constant in experiments, the SPR signal is directly dependent on the change of the refractive index of the medium on the sensor side of the SPR surface.

2.1.1 Surface Plasmons

Surface plasmons (SP) are phenomenon that the electromagnetic waves is evanescent in interaction processes between conduction electrons and electromagnetic radiation at the metal film (Economou 1969). The magnitude of the wavevector of the surface plasmon is related to the electric permittivity of both the dielectric medium and the metal film. We will examine the electromagnetic behavior of metals at optical wavelengths. On the reflection site, a metal film is covered by prism. In this case, the metal film exhibits the SPR signal at appropriate combination of wavelengths and reflected angle. The incident light is absorbed by metal film and its energy is transferred to the electrons, resonating at surface plasmon frequency.

2.1.2 Dielectric Function of Metals

In optics research, metals have not been much interesting. It is a common that metals don't give optical waves a chance to pass through. In addition, they mostly reflect off electromagnetic waves at a large spectrum ranging from microwave up to visible wavelengths. In general, they are used to prevent light escaping from the light source. The metal surfaces act like good or perfect conductors for low frequency regime. When the electromagnetic waves with low frequencies hit on the metal surface, they will reflect back with insignificant low energies loss due to little portion drilling into the metal surface. However, when the electromagnetic waves are in visible regime, higher portion can penetrate into the metal surface, leading to more energy loss (Earp 1998) and when in ultraviolet regime, the metal film behaves like dielectrics and becomes transparent at a definite frequency offset. These highly dispersive characteristics of the metals can be described by the so-called Lorentz-Drude model.

Lorentz-Drude model is based on viewpoint of plasma model that in a metal there are free electrons moving along the positive nuclei background. When EM waves impinge on the metal, they will induce free electrons oscillating on the metal surface. However, their oscillations are damped due to collision between electrons with a frequency $\gamma = 1/\tau$, where τ is the free-electron duration time. At room temperature, τ is on the order of 10 fs, which corresponds to collision frequency of 10^{14} collisions a second. In the plasma model, when the damped electron is subjected to an external electric field, its equation of motion is in the following form:

$$m\ddot{r} + m\gamma\dot{r} = -eE. \tag{2.1}$$

For the applied EM wave $E(t) = E_0 e^{-i\omega t}$, the solution supposed to be $r(t) = r_0 e^{-i\omega t}$ yields

$$r(t) = \frac{(eE_0/m)e^{-i\omega t}}{\omega^2 + i\gamma\omega}. \tag{2.2}$$

Oscillation can induce a dipole moment $p = -er$ with polarization density given by

$$P = -\mathrm{ne}r(t) = -\frac{(ne^2E_0/m)e^{-i\omega t}}{\omega^2 + i\gamma\omega}. \tag{2.3}$$

From Maxwell's equations, the electric displacement $D = \varepsilon_0 E + P$. Hence, one has

$$D = \varepsilon_0 \left(1 - \frac{\omega_p^2}{\omega^2 - i\gamma\omega}\right) E, \tag{2.4}$$

where $\omega_p^2 = \frac{ne^2}{\varepsilon_0 m}$ is the square of plasma frequency of free electron. For metal, its complex dielectric function $\varepsilon(\omega) = \varepsilon_r(\omega) + i\varepsilon_i(\omega)$ is

$$\varepsilon(\omega) = 1 - \frac{\omega_p^2}{\omega^2 - i\gamma\omega}, \tag{2.5}$$

Yielding the real and imaginary parts of $\varepsilon_{(\omega)}$ as follows:

$$\varepsilon_r(\omega) = 1 - \frac{\omega_p^2\tau^2}{1 + \omega^2\tau^2} \tag{2.6}$$

$$\varepsilon_i(\omega) = \frac{\omega_p^2 \tau}{\omega(1+\omega^2\tau^2)} \tag{2.7}$$

When working in a regime of frequency close to ω_p and $\omega\tau >> 1$, the imaginary part of the dielectric constant goes to zero. Within this approximation, the dielectric function of metal converges to

$$\varepsilon(\omega) = 1 - \frac{\omega_p^2}{\omega^2} \tag{2.8}$$

However, in the SP applications we used the Equation 2.5 to describe the dielectric function to parameterize the optical constants of metal (Dai 2012). The constants ω_p and γ are determined by fitting the Lorentz-Drude model to the experimental dielectric constant data (Atwater and Polman 2010). The dielectric functions for gold and silver films are depicted in Figure 2.1 (Gürel 2009).

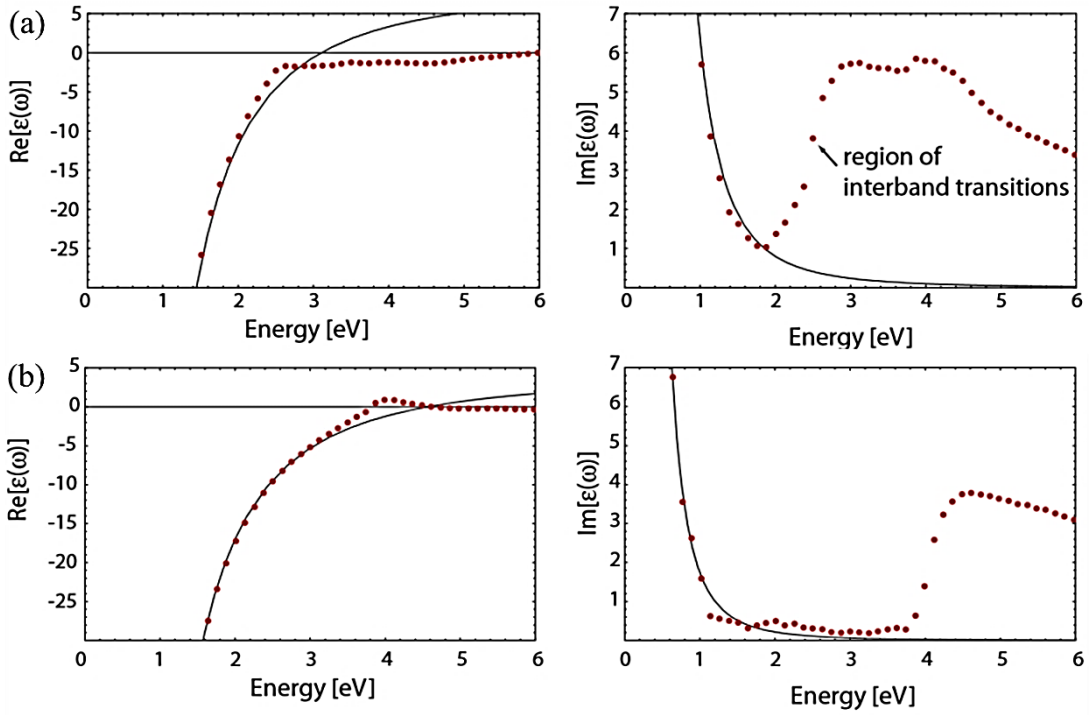

Figure 2.1 Dielectric functions of metal film gold (a) and silver (b) with respect to photon energy. Dotted lines are experimental data and curve-fitted lines by Lorentz-Drude models.

2.1.3 Surface Plasmons at Metal Dielectric Boundaries

Surface plasmon polaritons (SPPs) are electromagnetic excitations that propagate along interface between two mediums, dielectric and metal surface, and evanescently confined in the perpendicular direction. These EM waves at the interface arise via the electromagnetic fields coupling to oscillated spectrum of the electron plasma in metal (Maier 2007). In other words, dielectric interfaced to metal is capable to support the surface plasmon polaritons. Coherent longitudinal charge oscillations of conduction electrons in metal permit propagation at the interface of the surface plasmons. (Figure.2.2). The propagating wave caused by these oscillations has its maximum at the boundary and its amplitude decays proportional with its distance from the boundary (Gürel 2009).

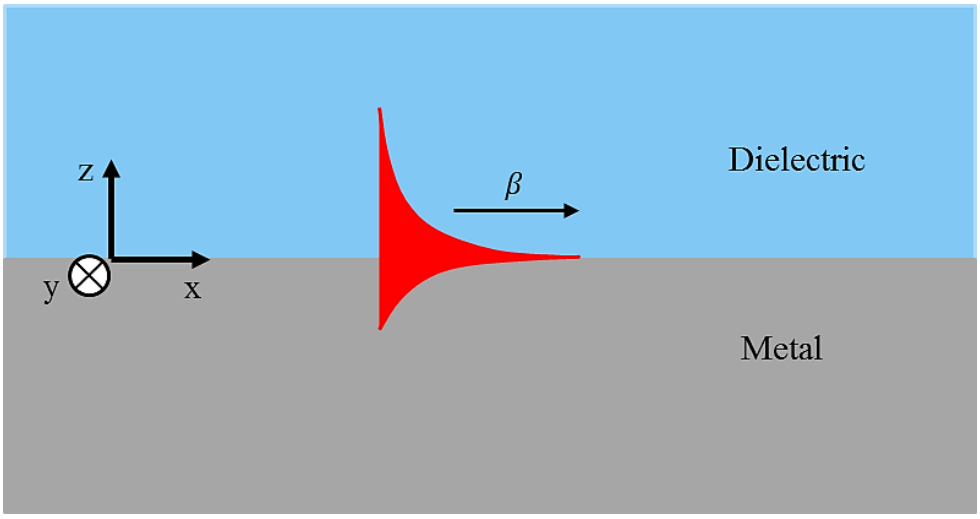

Figure 2.2 Schematic of a surface plasmon (SP) propagation at dielectric-metal interface in the x direction. The SP intensity on both sides of the interfaces decays exponentially from its the maximum. Theoretically, intensity drop inside metal is much faster than it does inside dielectric. The SP propagation is parallel to the interface.

The field distribution due to surface plasmons can be explained by solving Maxwell's equations that are composed of four fundamental equations in electromagnetic theory. In nonmagnetic and homogeneous medium the Maxwell's equations give rise to the scalar wave equation:

$$\vec{\nabla}^2 E(\vec{r},t) - \frac{\varepsilon_r}{c^2}\frac{\partial^2 E(\vec{r},t)}{\partial t^2} = 0. \tag{2.9}$$

As the electromagnetic wave is harmonically dependent on time, one can assume $E(\vec{r},t) = E(\vec{r})e^{-i\omega t}$. Substituting $E(\vec{r},t)$ into Equation 2.9, one obtains an equation so-called the Helmholtz eqation akin to the eigenvalue problem as follows:

$$\nabla^2 E(\vec{r}) + k_0^2 \varepsilon_r E(\vec{r}) = 0. \tag{2.10}$$

For the propagating waves of surface plasmon as shown in Fig 2.2, one can also assume $E(\vec{r}) = E(z)e^{i\beta x}$, where $\beta = k_{sp}$ is the surface plasmon propagation constant along x direction. After substituting $E(\vec{r})$ back into Equation 2.10, one yields

$$\frac{\partial^2 E(z)}{\partial z^2} + (k_0^2 \varepsilon_r - \beta^2)E(z) = 0. \tag{2.11}$$

$E(z)$ remains the wave propagation equation. Note that this wave propagation equation also holds for magnetic field (H field). However, we still do not have an explicit equation for describing surface plasmon.

From the Maxwell's curl equations of electric and magnetic fields,

$$\nabla \times E = -\frac{\partial B}{\partial t}, \tag{2.12}$$

and

$$\nabla \times H = J_{ext} + \frac{\partial E}{\partial t}, \tag{2.13}$$

it is assumed that there is no current density induced at surface due to the interaction of electromagnetic field with materials. For any oscillatory field in time the action of

the operator $\frac{\partial}{\partial t}$ on the field gives rise to multiplication of $-i\omega$ to the field. For homogeneity of field along y-axis, e.g. $E(\vec{x}) = E(z)e^{i\beta x}$, one yields $\frac{\partial E}{\partial y} = 0$. Finally, one obtains a set of six scalar equations from (2.13) and (2.14) as the follows:

$$\frac{\partial H_y}{\partial z} = \omega\epsilon_0\varepsilon_r E_x, \tag{2.14}$$

$$\frac{\partial H_x}{\partial z} - i\beta H_z = -i\omega\epsilon_0\varepsilon_r E_y, \tag{2.15}$$

$$i\beta H_y = -i\omega\epsilon_0\varepsilon_r E_z, \tag{2.16}$$

$$\frac{\partial E_y}{\partial z} = -i\omega\mu_0 H_x, \tag{2.17}$$

$$i\beta E_z - \frac{\partial E_x}{\partial z} = -i\omega\mu_0 H_y, \tag{2.18}$$

$$\beta E_y = \omega\mu_0 H_z. \tag{2.19}$$

The above six scalar field equations have to be imposed by transverse properties of electromagnetic waves, either the transverse electric (TE or s-polarized) or transverse magnetic (TM or p-polarized) modes. For TE mode only nonzero components are E_y, H_x and H_z and for TM mode only nonzero components are H_y, E_x and E_z. From equations (2.14)-(2.19), in case of TE mode, one yields as follows:

$$H_x = i\frac{1}{\omega\mu_0}\frac{\partial E_y}{\partial z}, \tag{2.20}$$

$$H_z = \frac{\beta}{\omega\mu_0}E_y, \tag{2.21}$$

$$\frac{\partial^2 E_y}{\partial z^2} + (k_0^2\varepsilon_r - \beta^2)E_y = 0 \tag{2.22}$$

and in case of TM mode as follows:

$$E_x = -i\frac{1}{\omega\varepsilon_0\varepsilon}\frac{\partial H_y}{\partial z}, \tag{2.23}$$

$$E_z = -\frac{\beta}{\omega\varepsilon_0\varepsilon} H_y, \tag{2.24}$$

$$\frac{\partial^2 H_y}{\partial z^2} + (k_0^2\varepsilon_r - \beta^2)H_y = 0. \tag{2.25}$$

To investigate the surface plasmon propagating along a single metal thin layer coated with a dielectric one these basic equations have to be used for matching the electric and magnetic fields at the dielectric-metal interface. It is common to suppose that the field is uniform in y-axis, decays in z-direction and propagates along x-axis, i.e., $E(\vec{r}) = Ae^{-kz}e^{i\beta x}$. These assumptions also hold for the *H* field. In case of a TM wave incident on the interface above z > 0 in the dielectric layer, one has as follows:

$$H_y(x,z) = A_d e^{-k_d z} e^{i\beta x}, \tag{2.26}$$

$$E_x(x,z) = iA_d \frac{1}{\omega\varepsilon_0\varepsilon_d} k_d e^{-k_d z} e^{i\beta x}, \tag{2.27}$$

$$E_z(x,z) = -A_d \frac{\beta}{\omega\varepsilon_0\varepsilon_d} e^{i\beta x} e^{-k_d z}. \tag{2.28}$$

Similarly, for z < 0 in the metal layer, one has as follows:

$$H_y(x,z) = A_m e^{i\beta x} e^{-k_m z}, \tag{2.29}$$

$$E_x(x,z) = -iA_m \frac{1}{\omega\varepsilon_0\varepsilon_m} k_m e^{i\beta x} e^{-k_m z}, \tag{2.30}$$

$$E_z(x,z) = -A_m \frac{\beta}{\omega\varepsilon_0\varepsilon_m} e^{i\beta x} e^{-k_m z}. \tag{2.31}$$

Continuity of H_y at the metal-dielectric boundary requires that $A_m = A_d$. Similarly, for continuity of the electric displacement at the interface requires that $\varepsilon_d E_{z,d} = \varepsilon_m E_{z,m}$. Combining these two continuities yields

$$\frac{k_d}{k_m} = -\frac{\varepsilon_d}{\varepsilon_m}. \tag{2.32}$$

This equation states that surface plasmons are sustained by the interfaces where the electric permittivities of the two layers have opposite signs, i.e. conductor-insulator interfaces. With respect to our metal-dielectric interface, this result does not seem surprising at all. We also know that H_y satisfies the eigenvalue (2.25) for both z < 0 and z > 0.

$$k_d^2 = \beta^2 - k_0^2 \epsilon_d \,, \tag{2.33}$$

$$k_m^2 = \beta^2 - k_0^2 \epsilon_m \,. \tag{2.34}$$

Finally, when substituting (2.32) into (2.33) and (2.34), one arrives at the dispersion relation of surface plasmons at a metal-dielectric interface

$$\beta = k_0 \sqrt{\frac{\varepsilon_m \varepsilon_d}{\varepsilon_m + \varepsilon_d}} \,. \tag{2.35}$$

For metal $\varepsilon_m = \varepsilon_m' + i\varepsilon_m''$ and $|\varepsilon_m'| \gg |\varepsilon_m''|$, (2.35) can be written as

$$\beta = \beta' + i\beta'' = k_0 \sqrt{\frac{\varepsilon_m' \varepsilon_d}{\varepsilon_m' + \varepsilon_d}} + i k_0 \frac{\varepsilon_m''}{2(\varepsilon_m')^2} \left(\frac{\varepsilon_m' \varepsilon_d}{\varepsilon_m' + \varepsilon_d} \right)^{3/2}. \tag{2.36}$$

Where β' corresponds to the real wavevector of surface plasmons and β″ represents the decay of SPPs propagating at the interface due to the energy loss in the metal.

Up to this point, dispersion relation of surface plasmon at a metal dielectric interface is derived for TM mode. Next the TE modes will be investigated to see whether there is any interesting result. For the same geometry the electric and magnetic fields in TE mode for z > 0 (in the dielectric) are

$$E_y(z) = A_d e^{i\beta x} e^{-k_d z}, \tag{2.37}$$

$$H_x(z) = -iA_d \frac{1}{\omega \varepsilon_0 \varepsilon_d} k_d e^{i\beta x} e^{-k_d z}, \tag{2.38}$$

$$H_z(z) = A_d \frac{\beta}{\omega \varepsilon_0 \varepsilon_m} e^{i\beta x} e^{-k_m z}. \tag{2.39}$$

and for z < 0 (on the metal)

$$E_y(z) = A_m e^{i\beta x} e^{-k_m z}, \tag{2.40}$$

$$H_x(z) = -iA_m \frac{1}{\omega\mu_0} k_m e^{i\beta x} e^{-k_m z}, \tag{2.41}$$

$$H_z(z) = -A_m \frac{\beta}{\omega\mu_0} e^{i\beta x} e^{-k_m z}. \tag{2.42}$$

From these two sets of equations, (2.37)-(2.39) and (2.40)-(2.42), the continuity of E_y at the interface again requires that $A_m = A_d$. Since continuity of H_x at the interface results in

$$A_m(k_1 + k_2) = 0, \tag{2.43}$$

which satisfies only when $A_m = A_d = 0$. Consequently, the surface plasmon modes can occur only by the EM waves in the TM mode while ones in TE mode cannot excite any surface plasmon.

Dispersion relation (2.35) drew in Figure 2.3 gives a significant information about behavior of SPPs. As Re (ε_m) or $\varepsilon'_m < 0$, but for realization of (2.36) in real life one needs a positive $\beta' = k_0\sqrt{\frac{\varepsilon'_m\varepsilon_d}{\varepsilon'_m+\varepsilon_d}}$ values, i.e., square-root needs to be positive. If $\varepsilon'_m < -\varepsilon_d$, then $\sqrt{\frac{\varepsilon'_m\varepsilon_d}{\varepsilon'_m+\varepsilon_d}} > 1$. The last inequality including with (2.32) mathematically proves that the wavevector of a surface plasmon at a metal-dielectric interface is higher than that of the wave propagating in the dielectric. Therefore, one can concludes that it is not possible to directly couple light from air to a propagating SPP. Figure 2.3 shows the dispersion of SPPs agrees with the conclusion. For any frequency ω, the surface plasmon wavevector β always lies below the light line which is the dispersion relation of the EM waves in air. Since there is no intersection point between the surface plasmon dispersion and the light line, coupling of SPP with light cannot occur. However, there are some tricks to create SPP by increasing the wavevector of incoming light that can generate surface

plasmon in the metal coupling to the EM wave in the dielectric. In the following subsections, we will discuss two methods that can create surface plasmon polaritons.

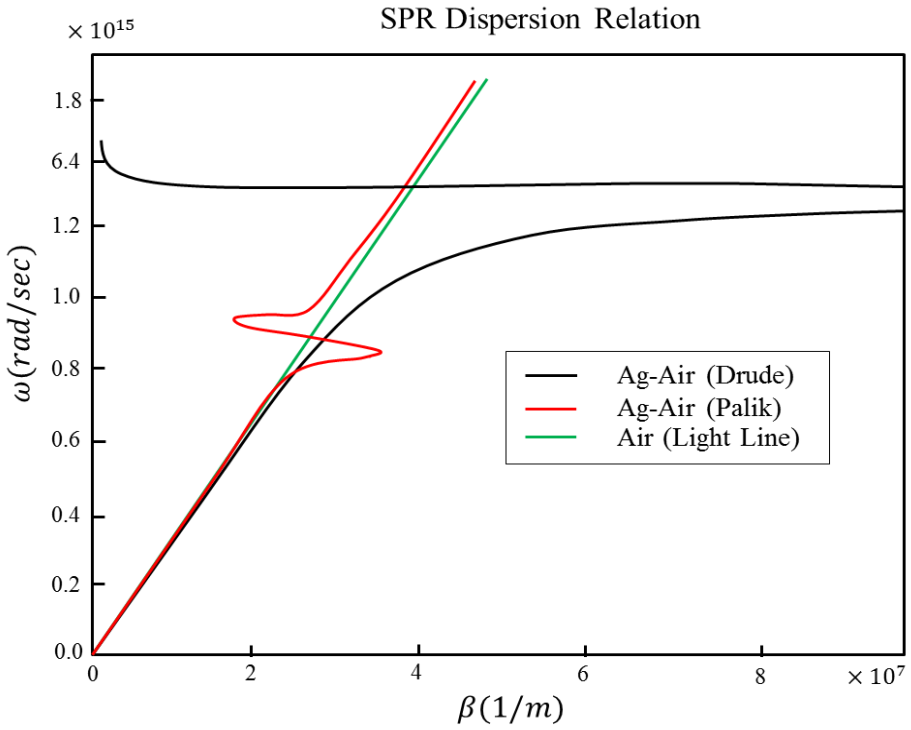

Figure 2.3 Dispersion relation for the surface plasmon polaritons at metal-dielectric Interfaces (Gürel 2009).

2.2 SPP Coupling Techniques

An important feature of SPPs is that, for a given angular frequency ω, an interaction between light line and surface plasmon dispersion results from the inborn bound nature of SPPs as an origin of the physical principles behind the expanded SPP force for the solid coupling amongst light and surface charges.

In general, an electromagnetic plane wave in TM mode impinging on a metal surface from the outside dielectric medium does not excite SPPs. For the excitation to happen in real situation, the wavevector of light needs to intercept the wavevector of the single interface SPP mode. Such an event happens just for $\omega \rightarrow 0$, since the SPP scattering asymptotically approaches the light line just for small angular

frequencies. Therefore, SPPs on a solitary metal-dielectric interface cannot be energized by light of any angular frequency unless uncommon stage coordinating methods such as crystal or grinding coupling are implemented (Ruppin and Boardman 1982; Kretschmann and Raether 1968; Otto 1968). Another technique to excite SPPs is by the end-fire coupling (Stegeman, Wallis, and Maradudin 1983), which depends on the spatial-mode coordinating rather than the stage coordinating.

2.2.1 ATR Prism Coupling

The most common method used for excitation of surface plasmons is the attenuated total reflection (ATR). Mainly, there are two configurations for the ATR, the Kretschmann geometry (Kretschmann and Raether 1968) and the Otto geometry (Otto 1968), depicted in Figures 2.4 (a) and (b), respectively. In both geometries, a prism of high dielectric constant ε_1 lies above a metal-dielectric (air) waveguide comprising of a thin metal film of dielectric constant ε_m and air of dielectric constant ε_2 ($\varepsilon_2 < \varepsilon_1$).

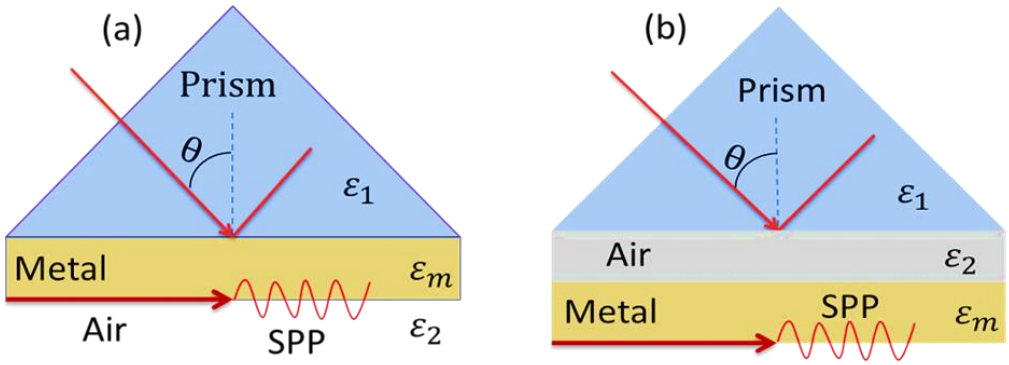

Figure 2.4 Two ATR geometries for prism coupling (a) Kretschmann and (b) Otto configurations.

The central thought is to send the light from a high refractive index prism to the thin metal film. When light enters the prism, its wavenumber becomes $k_p = k_0 n_p$. The light line of the prism can have an intersecting point with

the dispersive curve of surface plasmons on metal-air interface. This means that one can fulfill the fundamental condition to generate surface plasmons on metal-air interfaces by the EM wave of higher energy sent through a prism.

By ATR methods, the incident EM wave can be completely reflected from a prism-metal interface for Kretschmann geometry or from a prism-dielectric interface for Otto geometry. While it is being reflected, it enters into the thin layer of metal for a small depth. This infiltrated EM wave oscillates free electrons situated below metal surface generating an EM wave. The occurrence waves also cause electrons adjusting its oscillations until having reverberation or surface plasmon resonance. This happening is vital for the occurence EM wave propagating in the dielectric along the surface plasmon wave propagating in the metal at the metal-dielectric interface so-called surface plasmon polariton and yields the phase matching if $k_0 n_p \, sin(\theta) = k_{spp}$ holds. Therefore, the coupling condition for the geometry in Figure 2.4 is

$$k_0 n_p \, sin(\theta) = k_0 \sqrt{\frac{\varepsilon_m \varepsilon_2}{\varepsilon_m + \varepsilon_2}}, \tag{2.44}$$

which implies that the horizontal momentum of the incident wave in the prism matches to the momentum of the surface plasmon at metal-air interface.

2.2.2 Grating Coupling

Another method is to impinge an EM wave on the grinding metallic surface or grating (Gürel 2009). When the electromagnetic wave of wavevector k_0, whose wavelength is comparable to the grating period, is incident on the grating by an angle θ as depicted in Figure 2.5, it can be diffracted if the diffracted wavevector k_d satisfies

$$k_d = k_0 \, sin(\theta) + m\frac{2\pi}{\Lambda}, \tag{2.45}$$

where m is an integer denoting the diffraction order and Λ is the period of the grating. In this way, one can expand the momentum direction of the incident wave utilizing

the gratings. It brings up the idea of shining light from a dielectric specifically onto a metal grinding to energize surface plasmons at the dielectric-metal interface. The energy of diffracted light can be tuned by changing the angle θ and wavelength of the incident light, reverberation condition can be fulfilled and surface plasmons are energized as follows:

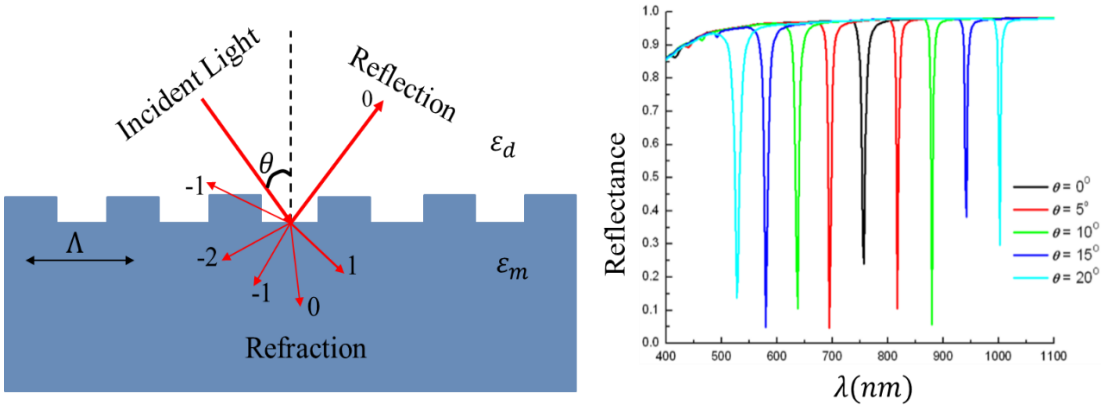

Figure 2.5 Schematic diagram of the metallic grating to generate SPR.

$$\frac{2\pi}{\lambda} n_d sin\theta + m\frac{2\pi}{\Lambda} = \frac{\omega}{c}\sqrt{\frac{\varepsilon_m \varepsilon_d}{\varepsilon_m + \varepsilon_d}}. \tag{2.46}$$

For prism coupling, the propagation direction of the surface plasmon is in the same direction as that of the k_x wavevector of the incident wave. However, for grating coupling other than the propagation direction of surface plasmon, there are orders of diffraction and these orders can couple to surface plasmons propagating along forward or backward directions. The change in forward or backward direction is represented by $sin\,\theta$ in (2.46). Thus, propagating surface plasmon resonances are shown as discrete dips in the reflectance spectrum in Figure 2.5.

2.3 Kretschmann Prism Arrangements

The Kretschmann prism arrangement is essentially a structure where a light ray is coupled into a SP mode that can exist on the surface of a thin metal film. Thin metal films are regularly utilized as SP support materials because of their optical properties and the relative simplicity with which they can be kept onto a substrate with a precise thickness. The bolster film is regularly stored onto a glass substrate that will be optically coupled to a waveguide. The fundamental criteria for a material to bolster SP waves are that the real part of the dielectric permittivity be negative. Some different materials that are reasonable bolster stages for SPR are copper, aluminum, palladium, platinum, nickel, cobalt, chromium, vanadium, tungsten, and some semi-transmitters (Ye and Zhang 2005). Metals are most usually utilized for SPR, and the remaining examinations will expect such a bolster surface for SP waves.

The physical environment in which the SP is made will extraordinarily adjust the coupling effectiveness of the light beam. In the Kretschmann course of action, the flimsy film supporting the SP is encompassed on both sides by dielectric materials. One of the dielectrics will be the waveguide, and the other will be the analyte test of interest.

The SP exists at the metal-example interface, where it is conceivable to have parts of an outer electric field from the creating light, E, present in both media. Caught inside the interface is the SP mode, which has an electric field that rots into the environment.

This surface mode is a charge thickness wave of electrons wavering on the metal film and will be affected by changes in the optical properties of the environment.

The component by which an electric field is coupled to the SP mode is appeared in Figure 2.6.

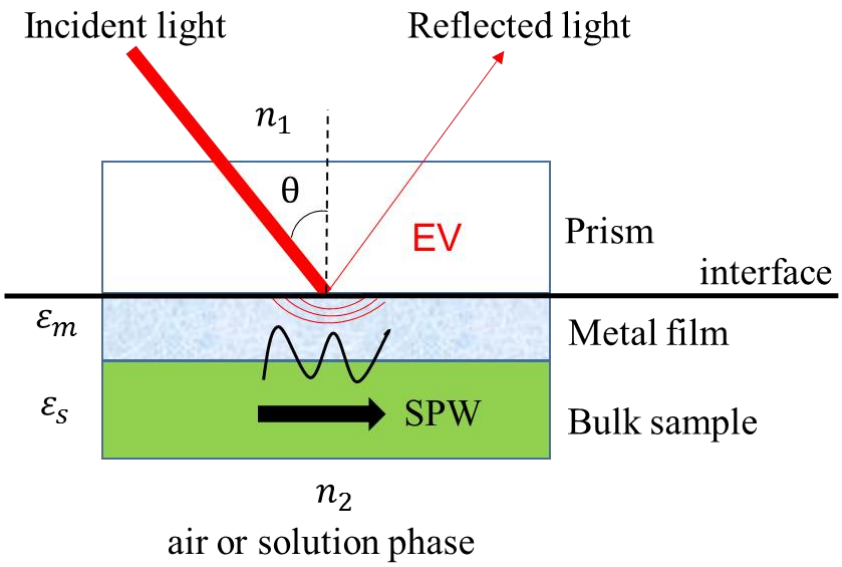

Figure 2.6 Schematic diagram of an SPR setup. SPW is surface plasma wave.

When the light source travels from medium 1 that is higher refractive index to the lower refractive index medium 2, the total internal reflection (TIR) can take place within medium 1 as long as the incident angle θ, is greater than the critical angle, θ_c, where $\sin(\theta_c) = n_2/n_1$. Evanescent waves are formed in the lower refractive index medium 2 under the condition of TIR. The dielectric permittivity ε is a dimensionless amount which is corresponding to the square of the refractive file of the material (inside the area of optical wavelengths). As the permittivity transforms this changes the coupling productivity of the light into the plasmon mode, which can be checked by watching the SP coupling angle, θ_{sp}- the occurrence light bar point giving most extreme SP coupling.

Total internal reflection is a phenomenon which occurs when a propagating wave strikes a medium boundary at an angle larger than a particular critical angle with respect to the normal to the surface. If the refractive index is lower on the other side of the boundary and the incident angle is greater than the critical angle, the wave cannot pass through and is entirely reflected.

The critical angle is the angle of incidence above which total internal reflection occurs. The angle of incidence is measured with respect to the normal at the

refractive boundary (see diagram illustrating Snell's law). Consider a light ray passing from glass into air. The light emanating from the interface is bent towards the glass. When the incident angle is increased sufficiently, the transmitted angle (in air) reaches 90 degrees. It is at this point no light is transmitted into air. The critical angle θ_c is given by Snell's law,

$$n_1 sin\,\theta_i = n_2 sin\,\theta_t \tag{2.47}$$

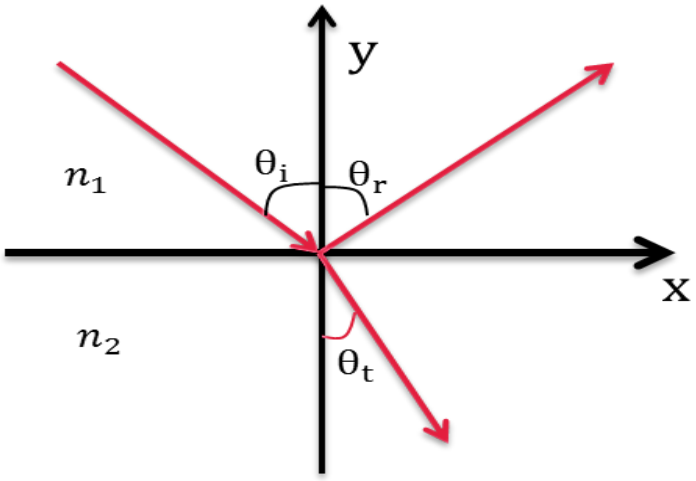

Figure 2.7 Illustration of Snell's law.

To find the critical angle, we firstly find the value of the incident angle θ_i, went the transmission angle θ_t is reaches 90 degrees and thus $\sin\,\theta_t = 1$. So the incident angle θ_i is equal to the critical angle θ_c, that following by equation

$$\theta_c = \theta_i = arcsin(\frac{n_2}{n_1}) \tag{2.48}$$

If the fraction $\frac{n_2}{n_1}$ is greater than 1, then arcsine is not defined meaning that total internal reflection does not occur even at very shallow or grazing incident angles. So the critical angle is only defined when $\frac{n_2}{n_1}$ is less than or equal to 1

2.4 Wavelength Modulation

SPR coupling can be accomplished through wavelength balance. In spite of the fact that not a quantitative articulation of the light wave vector, demonstrates that the light wave vector can be differed by changing the wavelength of the coupling light. The wavelength can be balanced by various methods, e.g., tunable diode lasers, color lasers, etc. These techniques have not yet accommodated the vast deviation in the light wavevector required for use in detecting applications covering a wide range of refractive index. The necessary dynamic range can be achieved through the use of a white light source.

2.5 Angle Modulation

The most common method used to vary the light wavevector for SPR sensor designs is angle modulation. Angle modulation is easy to implement and provides very accurate control over the incident light beam, leading to very good refractive index sensitivity. Experimentally, the Kretschmann design lends itself to a number of angle modulation schemes. A rotational stage can be used to move the entire sensor in relation to a fixed laser source. Alternatively, the sensor assembly can be mounted at the center of a goniometer with the laser source and detector mounted on swing arms. Both of these methods have been employed in this research. Commercial SPR units also employ angle modulation, but with a slightly different arrangement involving a photodiode array (PDA) for light detection. A range of angles is simultaneously launched into the waveguide. The PDA is used to measure the reflected light intensity for each angle and determine the angle of maximum coupling efficiency.

2.6 Momentum Resonance

Like all conversions, the phenomenon for a photon to generate surface plasmon at medium interface must conserve both energy and momentum in the system. Surface plasmons have a characteristic momentum determined by factors that include the nature of the conducting film and the properties of the medium on both sides of the film. The resonance occurs when the momentum of incident light hit on medium is equal to the momentum of the surface plasmons (Karlsson 2004). The momentum of the surface plasmons and photons can be described by a vector function possessing both direction and magnitude. As the wavelength or angle of the incident light changes, so does the relative magnitude of the components. However, the surface plasmon resonances are confined in the plane of the metal medium (gold film). For SPR it is only the vector component parallel to the surface that is significant. Therefore, the angle and the energy of the incident wave are unique. To create the SPR.

2.7 Evanescent Wave

At the total internal reflection, the reflected EM wave establishes an electric field propagating in the opposite side to the incident one at the interface. The surface plasmons create an occurrent non-propagating field attaching to the metal-film surface. This field is called the evanescent wave since its amplitude decreases exponentially with increasing depth from the interface, decaying over a distance by about the same order of light wavelength (Kogelnik and Shank 1972). Thus, the reflection depth of the evanescent wave is within ~300 nm of the sensor surface. The energy of the evanescent wave is dissipated as heat.

However, for the electromagnetic wave that passes through a surface medium depends on the properties of the medium, especially its refractive index. In a medium the light that possesses different wavelengths has different velocities and is seen refracted (Klozenberg, McNamara, and Thonemann 1965). Similary, the speed

of the surface plasmons is not a constant according to a change in the medium. This leads to a change in momentum as well as the angle of the incident light for occurrence of surface plasmon resonance.

2.8 Light Wave Coupling

The coupling of the light wave to the surface plasmons can be monitored in several ways. The most commonly used set-up is the angular SPR, also known as resonant angle SPR (De Vlaminck *et al*. 2007). The resonant angle can be measured very precise and is used for instance by BIACORE (Akimoto *et al*. 2000). Alternatively, for a fixed angle the wavelength of incident light can be varied until resonance occurs. This method is known as resonant wavelength SPR or spectral SPR, but it is not widely used. Another method is by detecting the phase shift of the light when the coupling between light and plasmons occur. In this method a reference beam must be used and requires a complex setup than other methods. However, it has a high sensitivity. The last SPR monitoring method to be mentioned is by measuring an intensity of the reflected light for SPR imaging (Caucheteur *et al*. 2011). This set-up makes it possible to simultaneously follow large numbers of SPR spots, and thereby increasing sample through put. Companies like IBIS Technologies and GWC Technologies produce instruments by this method.

CHAPTER 3

RESEARCH METHOLOGY

In this chapter, we present the theory and relevant research, modeling simulations by using COMSOL (version 4.2 update 3 licensed to the Prince of Songkla University), studying effects of physical parameters and analyzing computational results.

3.1 Studying the theory and relevant research

The surface plasmons can be explained as the collective oscillation of capacity electrons in a metal in response to the coming light. The resonance condition is established when the light frequency matches the natural frequency of surface electrons oscillating versus the restoring force due to positive nuclei. The common way to describe the existence and properties of surface plasmons is to treat each material layer as a homogeneous, continuum medium, in which the dielectric constant of materials is a complex-valued function with respect to wavelength. For the existence of the surface plasmons, the dielectric constant for the real part of the metal must be negative value and its magnitude must be greater than that of the dielectric. For study the relating theory of surface plasmon resonance occurs at two mediums interface to examine an antireflection at metal surface, the silver (Ag) slab was chosen to layer between the polycrystalline silicon dioxide (SiO_2) and air. The maximum energy transfer of the electromagnetic waves is probed by varying thickness of the Ag-slab. The frequency-dependent electric permittivity of SiO_2 is naturally described by Sellmeier formula (Malitson 1965).

$$\varepsilon_{\mathrm{SiO_2}} = 1 + \frac{0.6961663\lambda^2}{\lambda^2-(0.0684043)^2} + \frac{0.4079426\lambda^2}{\lambda^2-(0.1162414)^2} + \frac{0.8974794\lambda^2}{\lambda^2-(9.896161)^2}. \quad (3.1)$$

where λ is a wavelength expressed in micrometers. For the Ag-slab, its frequency-dependent electric permittivity based on the Lorentz-Drude model of free electrons is a complex number as follows:

$$\varepsilon_m = \varepsilon_\infty - \frac{\omega_p^2}{\omega^2 - i\Gamma_p\omega} + \sum_j \frac{f_j\omega_j^2}{\omega_j^2 - \omega^2 + i\Gamma_j\omega}. \quad (3.2)$$

Here ω_p is the plasma frequency, f_j is the strength of oscillator j , Γ_p is the plasma damping factor, and ω_j is its characteristic frequency. The conversion formula the wavelength of the light in (nm) and the photon frequency in (eV) is $\omega[eV] = 1239.8424/\lambda[nm]$.

And real and imaginary parts of ε_m are:

$$\varepsilon_m(r) = \varepsilon_\infty - \frac{\omega_p^2}{\omega^2 - \Gamma_p^2} + \sum_j \frac{f_j\omega_j^2\left(\omega_j^2 - \omega^2\right)}{\left(\omega_j^2 - \omega^2\right)^2 + \Gamma_j^2\omega^2}, \quad (3.3)$$

$$\varepsilon_m(i) = \frac{\Gamma_p\omega_p^2}{\omega^3 - \Gamma_p^2\omega} + \sum_j \frac{f_j\omega_j^2\Gamma_j\omega}{\left(\omega_j^2 - \omega^2\right)^2 + \Gamma_j^2\omega^2}. \quad (3.4)$$

where its plasma parameters and its first two-oscillator strengths that give the best fit with the experimental data in the visible and the IR region are given Table 3.1 (Shalabney and Abdulhalim 2012).

ε_∞	$\omega_p[eV]$	$\Gamma_p[eV]$	f_1	$\omega_1[eV]$	$\Gamma_1[eV]$	f_2	$\omega_2[eV]$	$\Gamma_2[eV]$
2.302	*8.807*	*0.082*	*0.439*	*4.602*	*0.761*	*1.098*	*6.008*	*2.393*

Table 3.1 Plasma parameters and the first two-oscillator strengths of silver.

3.2 Modeling for calculations using COMSOL

COMSOL Multiphysics (version 4.2 update 3 licensed to the Prince of Songkla University) was used for simulating nanomaterial**.** COMSOL basically follows Maxwell's equations which were described in the previous chapter, and they use finite difference methods, more flexible with respect to the geometry and is a numerical technique for finding approximate solutions to boundary value problems for partial differential equations.

3.2.1 Optimize Ag layer thickness for SiO_2-Ag-Air Coupler

For this model of structure in which a thin metal (Ag) layer is sandwiched between two mediums are Silicon dioxide (SiO_2) and Air layer and used the Floquet boundary condition (B.C.) and port (active and passive) in similar to Kretschmann configuration as shown in Figure 3.1.

To solve for the electric and magnetic fields by finite-element method implemented in COMSOL Multiphysics (version 4.2 update 3 licensed to the Prince of Songkla University), all two-dimensional physical domains comprising of SiO_2, Ag and air layers, whose width is 580 nm, were firstly created as shown in Figure 3.2(a), and triangular-meshed as shown in Figure 3.2(b).

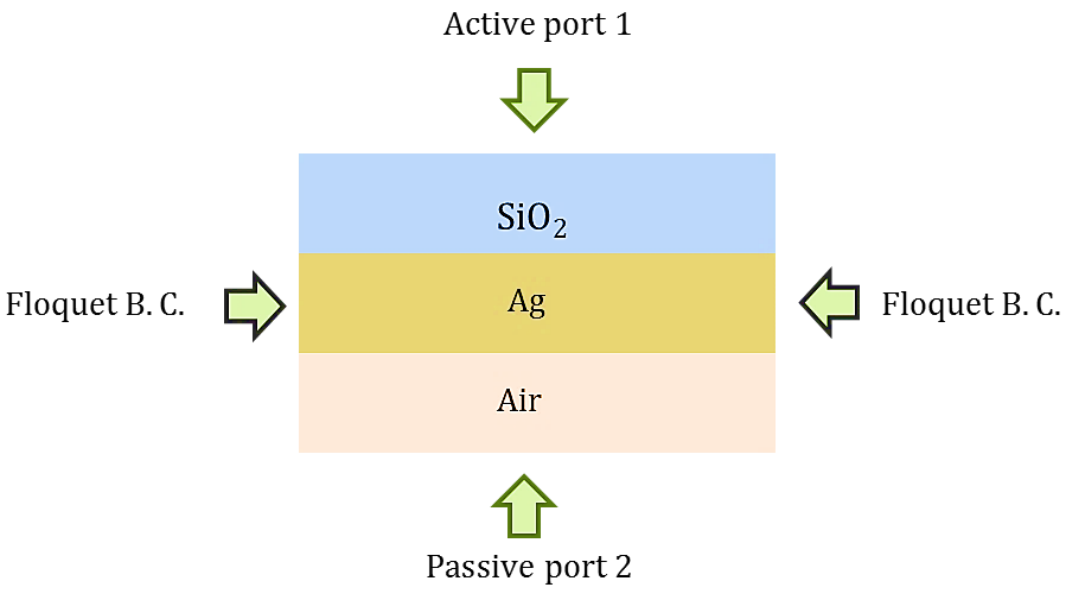

Figure 3.1 Model geometry of a SiO_2-Ag-Air coupler in Kretschmann configuration.

The height of SiO_2 and air layers is two times of their width. The SiO_2 and air domains were set to be active and passive ports, respectively. Other than the smooth surface of Ag-slab, a rough surface of grating type in an active and a passive port was also constructed for a comparative study. In numerical calculation, the momentum component of the electric field parallel to both SiO_2–Ag and Ag–air interfaces is preserved, i.e., and satisfies the Floquet periodicity.

$$k_{1x} = k_{2x} = k_{3x} = k_0\sqrt{\varepsilon_{SiO2}}\,\sin\theta \tag{3.5}$$

$$k_{1y} = -k_0\sqrt{\varepsilon_{SiO_2}}\,\cos\theta \tag{3.6}$$

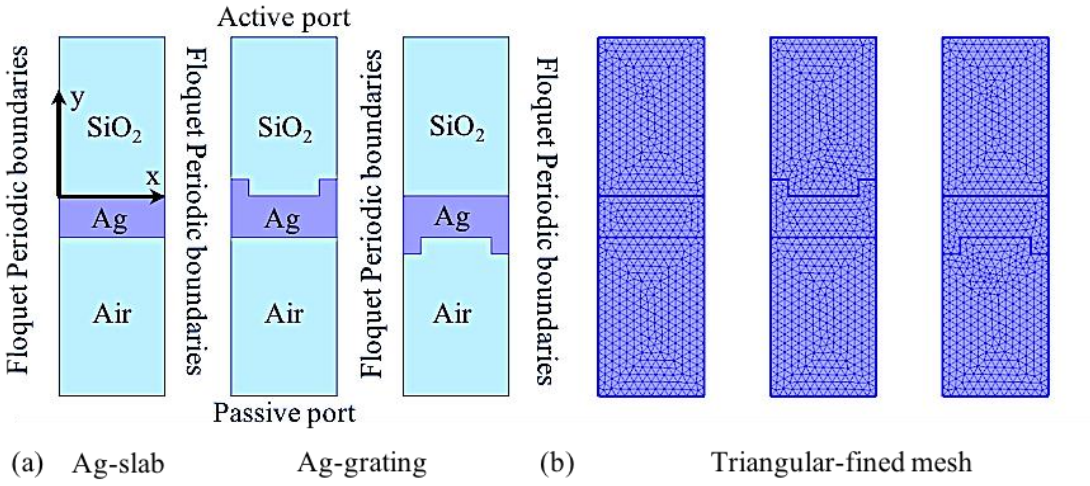

Figure 3.2 Two-dimensional physical domains of the SiO_2–Ag–air coupler.

The components of wave vectors in Ag layer k_{2y} and in air layer k_{3y} in y-direction yield the following equations:

$$k_{2y} = \sqrt{k_0^2 \varepsilon_m - k_{1x}^2}, \tag{3.7}$$

$$k_{3y} = \sqrt{k_0^2 \varepsilon_{Air} - k_{1x}^2} \tag{3.8}$$

For the SiO_2–Ag–air coupler, its reflection R for p-polarized light is quantitatively described by the well-known Fresnel's equation as follows (Raether 1988).

$$R = \left| \frac{r_{12}^p + r_{23}^p exp[2ik_{2y}d]}{1 + r_{12}^p r_{23}^p exp[2ik_{2y}d]} \right|^2, \tag{3.9}$$

$$r_{ij}^p = \left(\frac{k_{iy}}{\varepsilon_i} - \frac{k_{jy}}{\varepsilon_j} \right) \Big/ \left(\frac{k_{iy}}{\varepsilon_i} + \frac{k_{jy}}{\varepsilon_j} \right) \quad i, j = 1,2,3, \tag{3.10}$$

where 1, 2 and 3 represent SiO_2, Ag and air, respectively, and d is the Ag-slab thickness. When the electromagnetic wave is incident on the Ag surface, some part of its energy is absorbed by the Ag slab and the rest is transmitted to the air layer. Hence, the energy of coupler system is conserved, i.e.

3.2.2 Optimize Ag distance for plasmonic Solar Cell

Plasmonic light trapping via metallic nanostructures supplement is of particular interest for enhancing the efficiency of thin film solar cells. For designed the structures of plasmonic solar cell can be integrated within three ways (Atwater 2007). For the first structure, the spherical metal nanoparticles (Ag) will be placed on the top and metal film at back surface of a solar cell as shown in figure 3.3, and then it can supplement absorption in the SiO_2 layer by scattering the incident light into it and reducing the reflection. Second structure, the metal nano-spheres can be embedded inside between the Silicon (Si) and SiO_2 surface as shown in figure 3.4. And for the third structure of plasmonic solar cell, the metal nanoparticles like grating couples films can be placed at the back surface of a plasmonic solar cell will see in Figure 3.5. In the case of a thin metal film, Surface Plasmon polarize are excited at the interface between the metal and SiO_2 film, which supplement the optical light intensity and also couple the incident wave into the guided modes of the thin SiO_2 film.

In our simulations of a plasmonic solar cell structure the parameters that used for all two-dimensional physical domains comprising of Air, SiO_2 , Ag and Si layers, whose width is 1000 nm, the radius of the metal Nano-sphere (Ag) 40 nm, the thickness of Si slab 80 nm, the high and width of the Ag grating are 20 nm and we also various the distances (d) of spherical metal nanoparticles and grating (150 nm-180 nm). However, for two-dimensional in this model by COMSOL multiphysics the Floquet periodic boundaries condition, active port and passive port have been used in our work. The Air and Ag domains we were set to be active and passive ports, as shown in figure 3.3 and 3.5). Exception in figure 3.4), were set the Si domain to be a passive port, due to the Ag domain embedded inside between the SiO_2 and Si surface of a solar cell structure. Moreover, we calculate the absorbance to find the resonance frequency of the system. The absorbance can be find by A =1-R-T, in which R and T represent reflectance and transmittance respectively.

R and T are calculated by performing surface integral of Poynting vector on the surface under the Ag reflector and on the interface between the SiO_2 and Si layer, as defined in (3.9), (3.10) respectively.

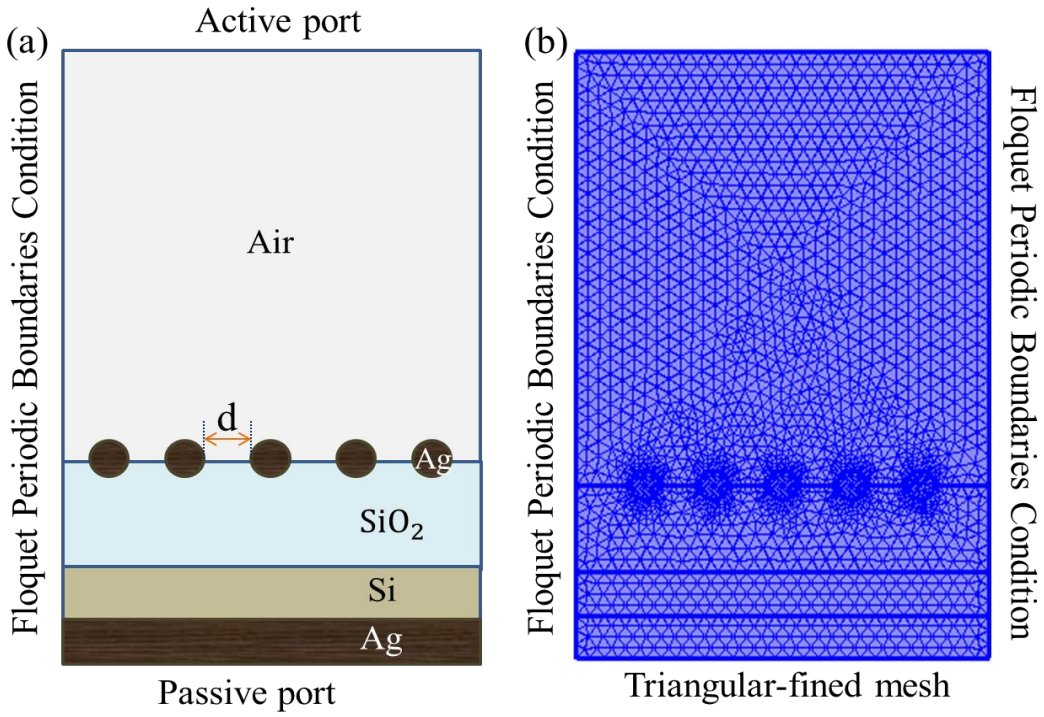

Figure 3.3 Schematic Diagram of two-dimensional physical domains of three plasmonic solar cell structures by COMSOL and Triangular-meshed. The metal Nano-spheres (Ag) are place at the top surface and metal film at back surface of a solar cell.

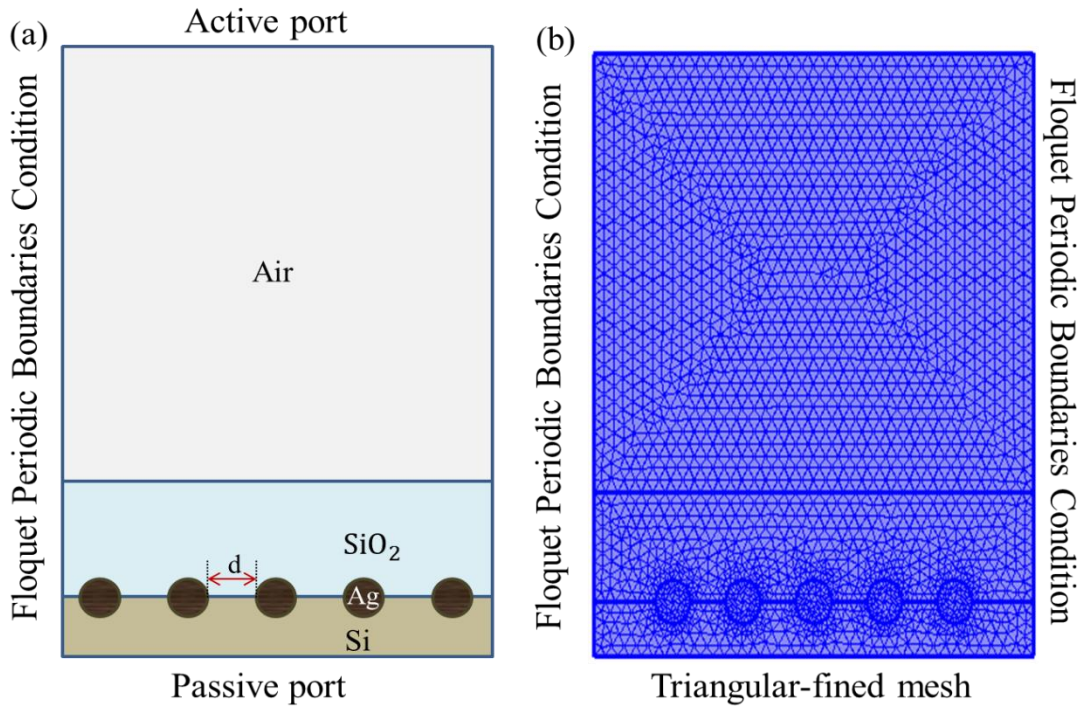

Figure 3.4 Metal Nano-Spheres (Ag) embedded inside between the Silicon (Si) and SiO_2 surface of a solar cell.

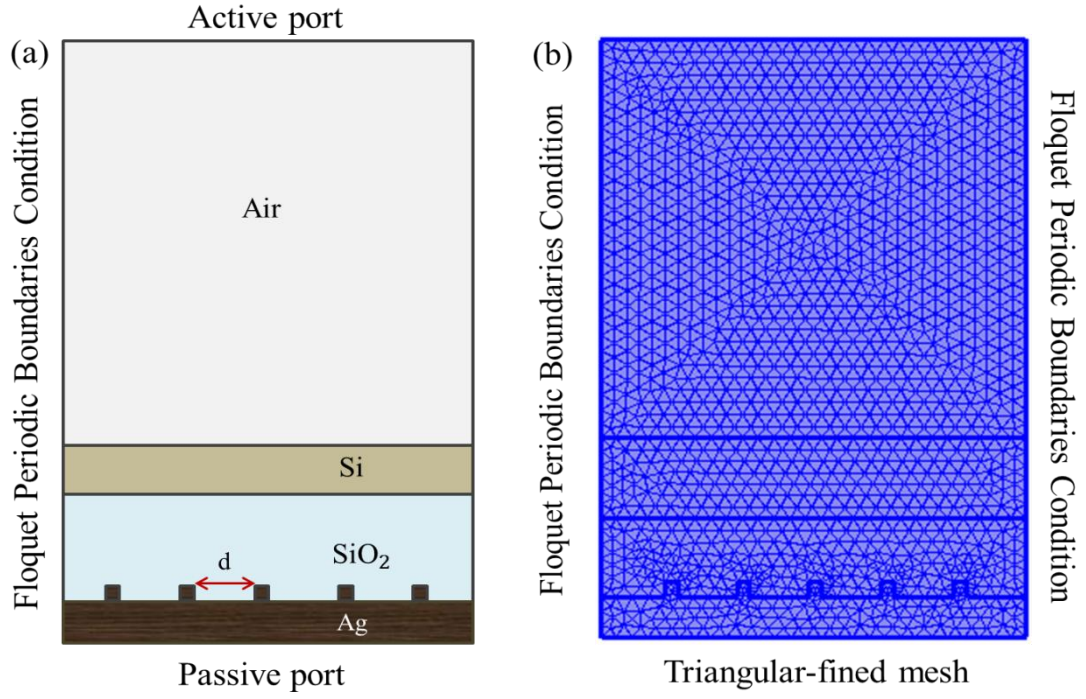

Figure 3.5 Metal nanoparticles or corrugated metal films at the back surface of a solar cell.

The reflection coefficient within the SiO_2 (labeled as 1) by

$$R = \frac{\int_{port_1}((E_{inc}-E_1)\cdot E_1)dA_1}{\int_{port_1}(E_1\cdot E_1^*)dA_1}, \tag{3.11}$$

and for the transmittance coefficient from the metal layer (labeled as 2) to SiO_2 by

$$T = \frac{\int_{port_2}(E_{inc}\cdot E_2^*)dA_1}{\int_{port_2}(E_2\cdot E_2^*)dA_2}. \tag{3.12}$$

The frequency-dependent electric permittivity of Si is naturally described by Sellmeier formula

$$\varepsilon_{Si} = 11.67316 + \frac{1}{\lambda^2} + \frac{0.00448233}{\lambda^2 - 1.108205^2} \tag{3.13}$$

The electromagnetic wave with its electric field $\vec{E}$ component in the frequency domain satisfies the Maxwell's equation to solved for in-plane vector and full field by

$$\vec{\nabla} \times \mu_r^{-1}\left(\vec{\nabla} \times \vec{E}\right) - k_0^2\left(\varepsilon_r - \frac{i\sigma}{\omega\varepsilon_0}\right)\vec{E} = 0 \tag{3.14}$$

In this study the electric field that is incident on the metal nanostructures at an angle θ is a p-polarized (TM) electromagnetic wave with its nonzero electric and magnetic components as follows, which is in x-z plane at $y = 0$

$$\vec{E} \sim \left(E_{1x}, E_{1y}, 0\right)e^{i(k_{1x}x + k_{1y}y) - i\omega t} \tag{3.15}$$

$$\vec{H} \sim (0, 0, H_{1z})e^{i(k_{1x}x + k_{1y}y) - i\omega t} \tag{3.16}$$

Where k_{1x} and k_{1y} are the wave vectors in the x- and y-components inside SiO_2 as defined in (3.5) and (3.6), respectively.

CHAPTER 4

RESULTS AND DISCUSSIONS

4.1 The results of the optimization Ag layer thickness for SiO_2-Ag-Air Coupler

The reflection response of the TM wave against the angle of incident light for computational solutions and the wavelength of the electric field at a fixed angle of incidence was firstly swept to obtain the wavelength that yields the lowest reflectance for different Ag thickness as shown in Figure 4.1(a). After that the incidence angle at the obtained wavelength was later swept for different Ag thickness as shown in Figure 4.2(b).

As shown in Figure 4.1(a), reflection and absorption of the electromagnetic wave at the silver surface for various thicknesses depends on the wavelength. The profiles of reflection coefficients for the Ag-slab thickness of more than 20 nm exhibits similar profile, pertaining a dip at a specific wavelength.

For the simulated results in this work, we validated the exactness of our results by comparing with the analytic theory and experimental results of surface plasmon excitation at metal-dielectric interface. Our simulated results agreed with the theory and experiment in both global and local characteristics. The common characteristics to locate SPR which occurs at two medium interfaces is by looking at the lowest reflection and the highest absorption at the metal surface. The minimum sharp dip of the reflection can be described by Fresnel's equations for the three-layer structure. The reflection and absorption depend on the combination of the wavelength, angle of incident light, and the thickness of the metal film (Sharma, Jha, and Gupta 2007).

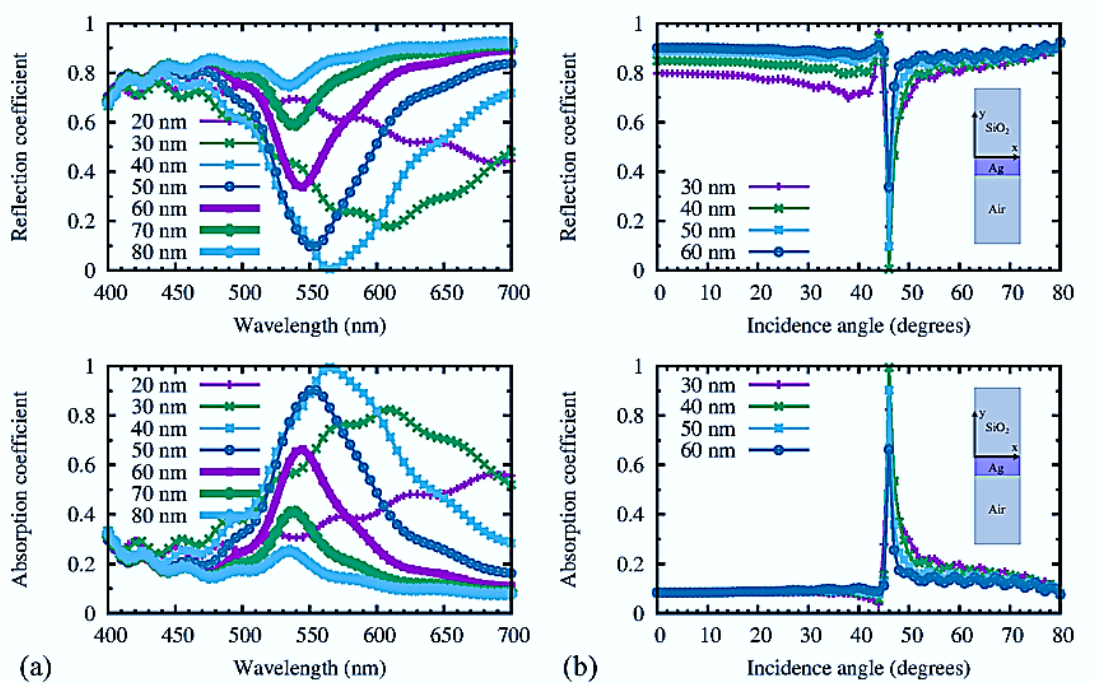

Figure 4.1 Reflection and absorption coefficients with respect to (a) wavelength and (b) incidence angle.

As shown in Figure 4.1(b), the profiles of reflection and absorption coefficients for various Ag-slab thicknesses also show similar characteristics, possessing the angle of critical reflection of 44° and the angle of surface plasmon resonance (or the Kretschmann's angle) of 46°. This angle of surface plasmon resonance is in agreement with the theoretical prediction from momentum matching condition (Raether 1988).

$$k_{sp} = k_0 \sqrt{\frac{Re[\varepsilon_m] \cdot \varepsilon_{air}}{Re[\varepsilon_m] + \varepsilon_{air}}} = k_0 \sqrt{\varepsilon_1}\, sin\, \theta_{sp} = k_{1x} \qquad (4.1)$$

The wavelengths that yield the lowest reflection coefficients for different Ag-slab thicknesses are summarized in Table 4.1. For thickness less than 70 nm, the thicker the Ag-slab, the shorter the wavelength.

Ag thickness (nm)	20	30	40	50	60	70	80
Wavelength (nm)	-	610	565	555	545	540	540

Table 4.1 Minimum of a reflection coefficient and the corresponding wavelength for different Ag thicknesses.

At the angle of surface plasmon resonance, the thickness of the Ag-slab of 40 nm possesses most antireflectance. The differences between electric field norms of the reflected waves at the angle of critical reflection of 44° and at the angle of surface plasmon resonance of 46° are shown in Figure 4.2(a) and 4.2(b), respectively. The reflected electric field norm at 44° is strong up to the order of 10^4 V/m; whereas, the one at 46° which is low to the order of a few tens V/m. From a viewpoint of wave optics, the light that passes through the SiO_2–Ag interface at the angle of surface plasmon resonance induces excitations at the Ag–air interface which radiate light back nearly in antiphase to the incident one, resulting in the destructive interference and yielding the value of R close to zero for the Ag-slab thickness of 40 nm. As the thickness of the Ag-slab increases, the antiphase back-radiated light decreases, resulting in the value of R getting off from zero.

In case that surface of the Ag-slab of 40 nm is rough akin to grating, the profiles of reflection and absorption coefficients for various heights h from the smooth Ag surface are shown in Figure 4. When grating is in the active port, for the height of 30 nm other than at the angle of surface plasmon resonance of 46° there are significant dips at the angle of 29°, 36°, and 56° that exhibit the destructive interference from the incident and back-scattered waves.

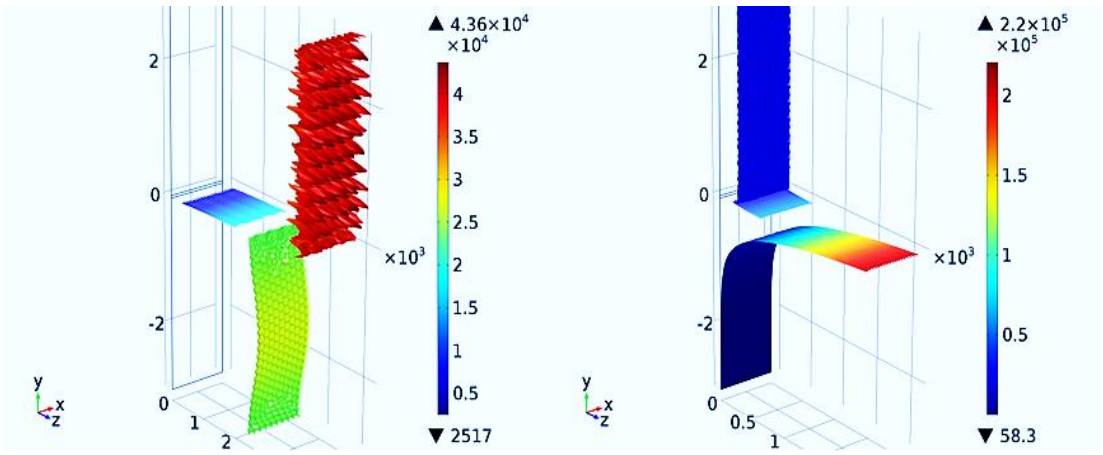

Figure 4.2 Electric field norm expressed as height in the z-axis at the angles of (a) critical reflection $\theta_c = 44^\circ$ and (b) surface plasmon resonance $\theta_{sp} = 46^\circ$.

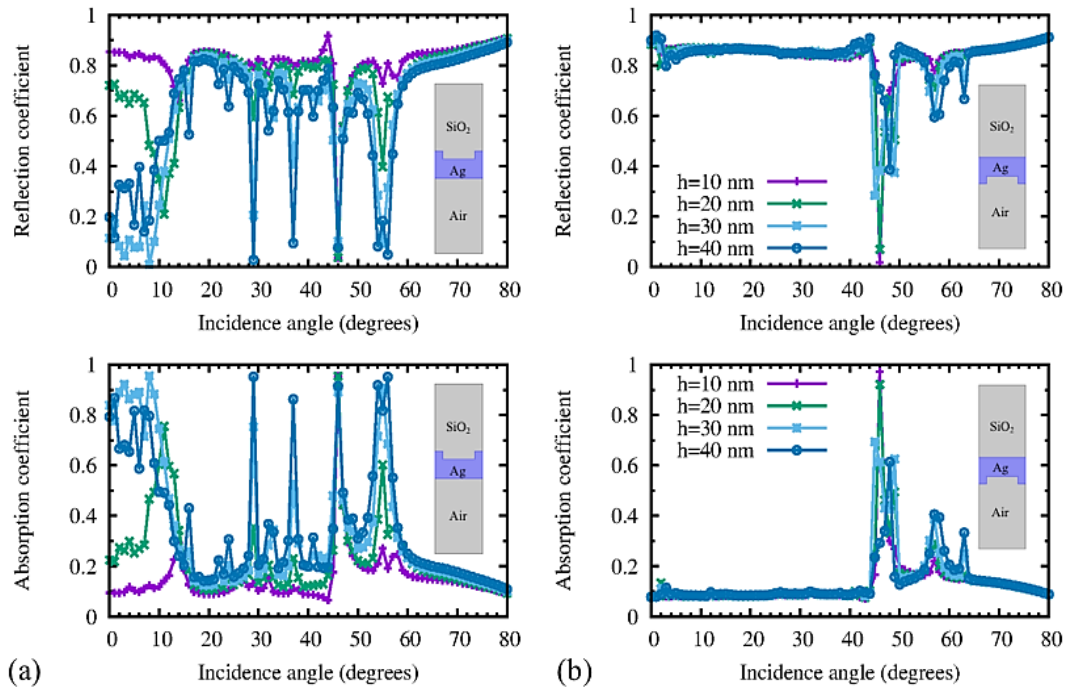

Figure 4.3 Reflection and absorption coefficients with respect to incidence angle for a rough surface of grating type in the (a) SiO_2 and (b) air layer.

When the gratings of different heights are in the passive port, there is no dip for the angles less than the angle of surface plasmon resonance of 46°. While above 46°, there are two minor dips at the angles of 57° and 64° due to out-of-phase interference between the incident and back-scattered waves.

4.2 The results of optimize Ag layer distances for a solar cell

The surface plasmon resonance is accompanied by strong absorption of absorber and the reflection resonance spectrum exhibit minimum at the resonance. The reflection coefficients response of the TM wave with the incident angle for optimization the plasmonic solar cell with metallic Nano-structure by COMSOL solutions are shown in figure 4.4a, 4.5a, and 4.6a,. The simulate results for the first structure that the spherical Nano-sphere on the top of solar cell structure in figure 4.4a, the profiles of reflection and absorption coefficients for various distances between of the spherical metal nanoparticles with incident wavelength 530nm, we can see the minimum sharp in reflectance angle of SP resonance occurs at an angle of 36°. For the angles less than angle of 36° of SP resonance will see the profiles of reflection coefficients also show similar characteristics at angles of 5° and 12°. In addition, for the angles more than angle of 36° of SP resonance and the distances of Ag nanoparticles less than 170nm the angles of reflectance resonances dip at angles of 44°, 60° and 70°, due to out-of-phase interference between the incident and back-scattered waves.

As shown in Figure 4.5a, and 4.6a, the dips in reflection resonance angle of SP resonance occur at an angle of 74° and 40° with incident wavelengths 650nm and 460nm respectively. The profile reflection coefficients also show similar characteristic with various spacing distances between nano-spheres and grating couples. In our simulations, we observed that the SP resonance angle doesn't change with respect to the spacing distances of Ag nanoparticles of 150 nm, 160 nm, 170 nm and 180 nm.

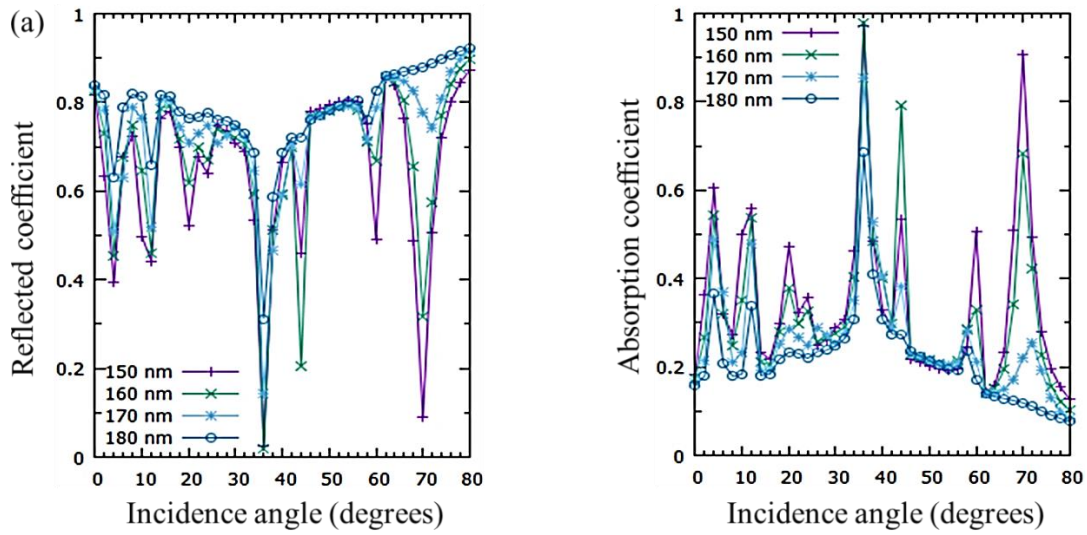

Figure 4.4 (a) Show the reflection and absorption coefficients with respect to incidence angles for Ag nano-spheres at front of a plasmonic solar cell structure.

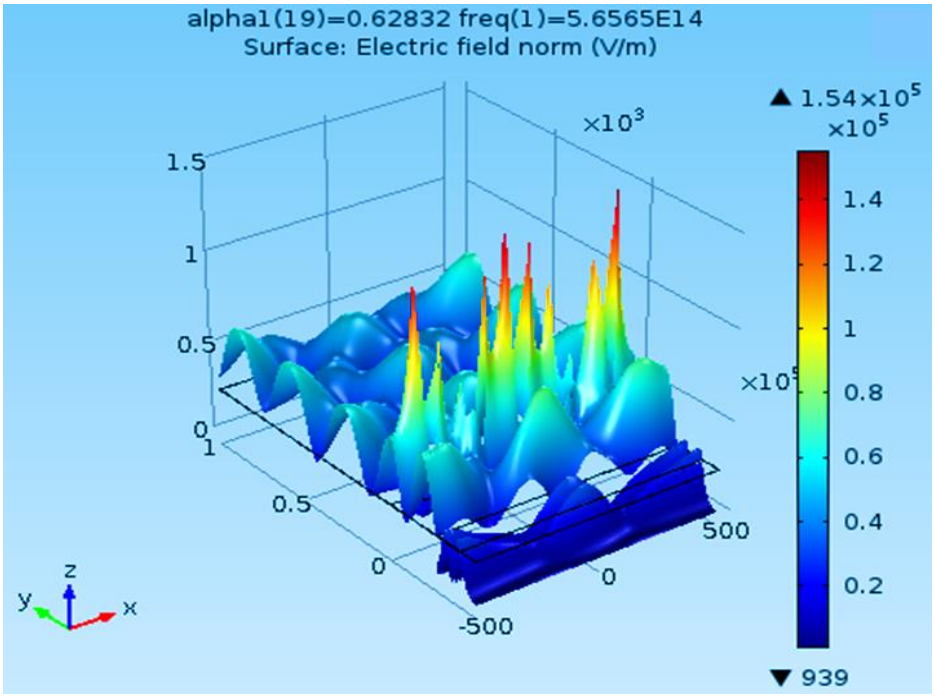

Figure 4.4 (b) Magnetic field norm expressed as height in the z-axis at the surface resonance angle $\theta_{sp} = 36^{\circ}$.

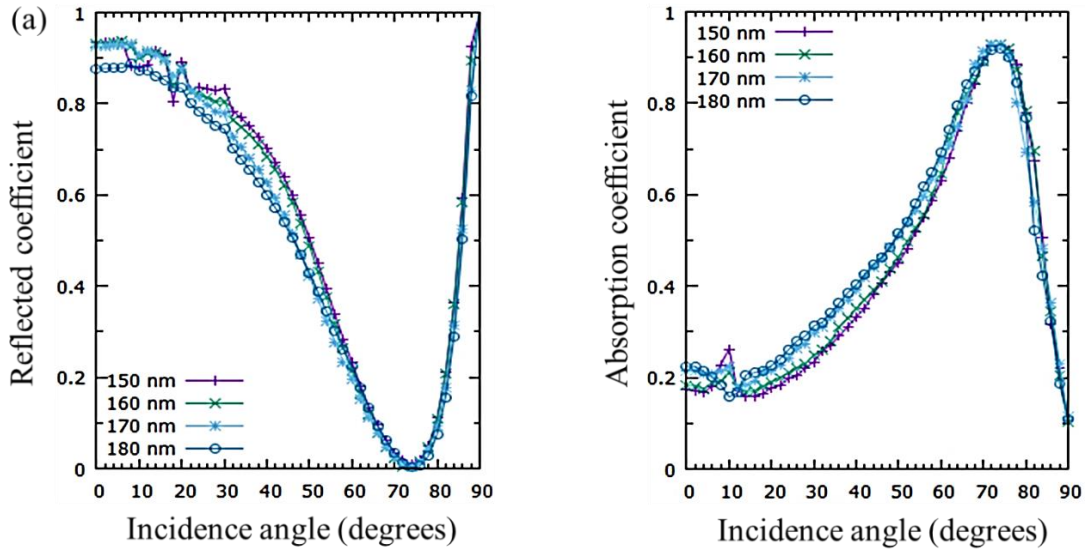

Figure 4.5 (a) The results of the coefficients with respect to incidence angles of second structure for the Ag spheres embedded inside between the Si and SiO_2 surface of a solar cell.

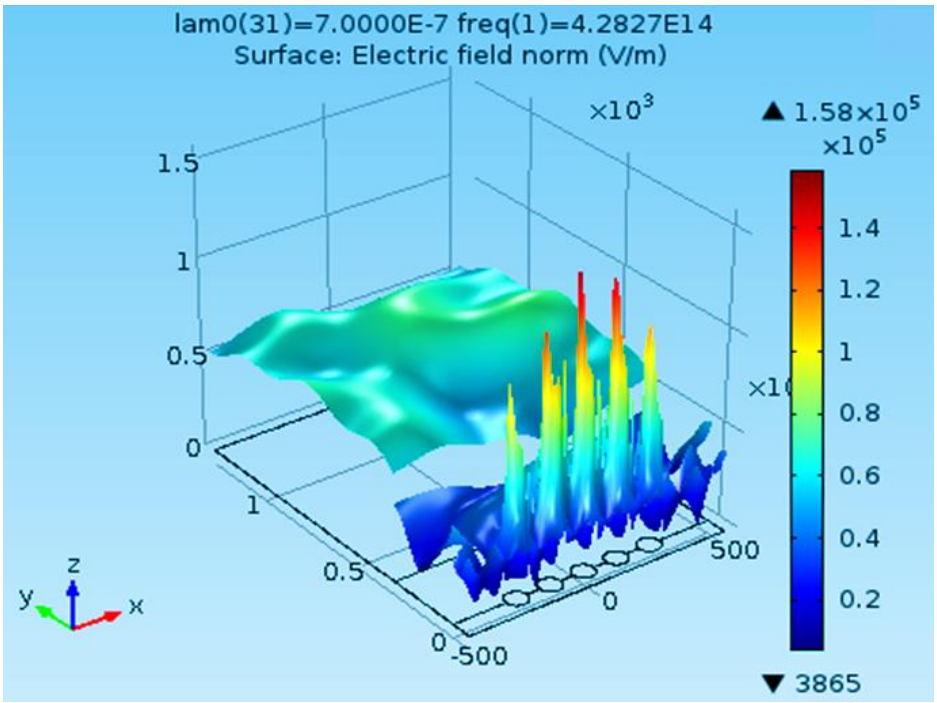

Figure 4.5 (b) Magnetic field norm expressed as height in the z-axis at the surface resonance angle $\theta_{sp} = 74^{\circ}$.

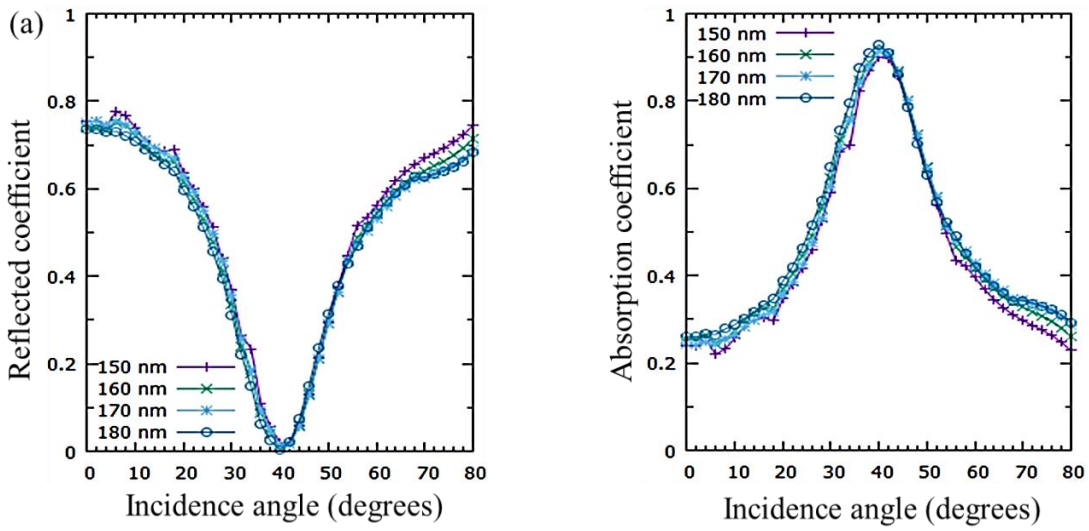

Figure 4.6 (a) The results of the coefficients with respect to incidence angles of second structure for the Ag grating couples at back surface of a solar cell.

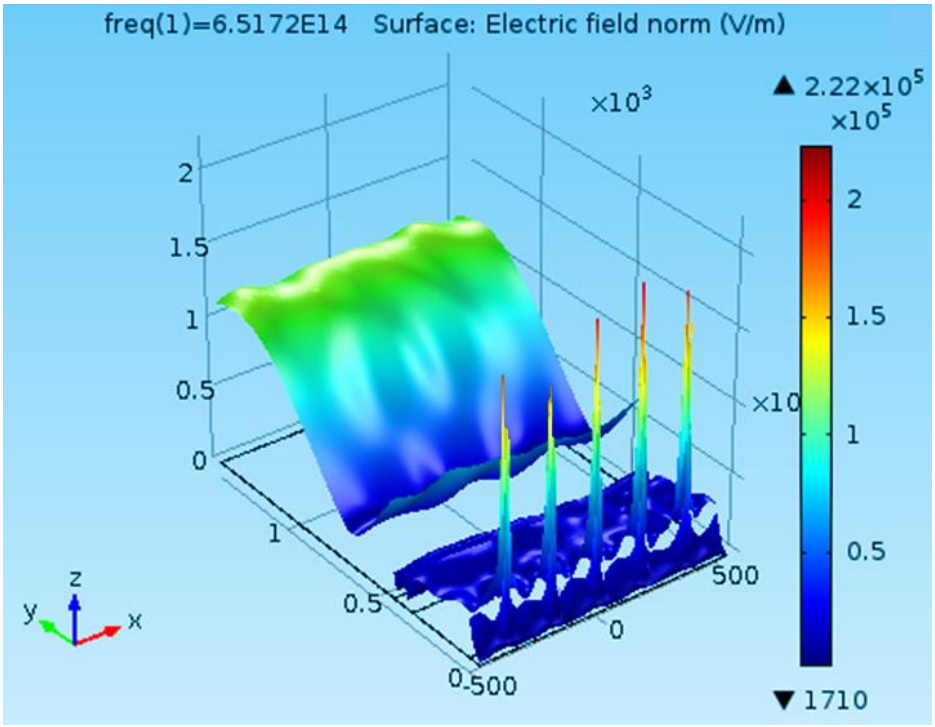

Figure 4.6 (b) Magnetic field norm expressed as height in the z-axis at the surface resonance angle $\theta_{sp} = 40^{\circ}$.

Figure 4.4b, 4.5b and 4.6b show the magnetic field distributions at their resonance angles, exhibiting high and sharp peaks at the metal-dielectric interfaces. These peaks are sensitive to the dielectric constant of the medium that is adjacent to metal. This sensitivity can be used for detecting chemical and biological agents that come to attach the dielectric surface and change its dielectric constant by an extremely small amount.

CHAPTER 5

CONCLUSION

This work presented the analysis of surface plasmon resonance using COMSOL Multiphysics. The most common configurations for surface plasmon propagating along the interface between metal and dielectric have been analyzed. The most prominent feature from spatial optimization is the maximum energy transfer of the electromagnetic waves, which is observed in dipping of total reflection off the metal surface at the Kretschmann's angle of incidence. In all two-dimensional physical domains comprising of SiO_2, Ag and air layers, their width is 580 nm. From the SiO_2-Ag-air coupler accompanying with the characteristics of electric permittivity in each layer, the electromagnetic field with wavelength of 565 nm yields the minimum reflection for the smooth surface of the Ag-slab with thickness of 40 nm. The minimum reflection and highest absorption coefficients that are explicitly seen in the electric field norm occurs at the angle of surface plasmon resonance of 46° in agreement with the theoretical calculation. For the rough surface of grating type with various heights, there are dips at the angles other than at the angle of surface plasmon resonance.

We systematically investigated the scattering and absorption of metallic nanoparticles embedded into surface layer of solar cell. Despite the fact that scattering can be enhanced by exciting plasmonic resonances, they are always accompanied with a strong absorption loss, which is a detrimental key factor limiting the solar cell performance. The reflection coefficients are calculated from the medium response to the TM wave at various incident angles for optimization of the plasmonic solar cell embedded with metallic nano-structure. For Ag nano-spheres imbedded on the top of a solar cell structure with incidence of the TM wave with wavelength of 530 nm, the minimum sharp dip in reflection coefficients exhibiting SP resonance occurs at an angle of 36° for the spacing distance between of the Ag nano-spheres of 160 nm. For the Ag spheres embedded inside between the Si and SiO_2 interface and for the Ag

grating at the bottom of a solar cell, the dips in reflection coefficients occurs at the angles of 74° and 40° with incident wavelengths 650nm and 460nm respectively. It is observed that for various spacing distances of either the Ag nano-sphere or the Ag grating of 150nm, 160nm, 170nm and 180nm there is no change in angle of SP resonance.

REFERENCES

Akimoto, T., S. Sasaki, K. Ikebukuro, and I. Karube. 2000. “Effect of Incident Angle of Light on Sensitivity and Detection Limit for Layers of Antibody with Surface Plasmon Resonance Spectroscopy.” *Biosensors & Bioelectronics* 15 (7–8): 355–62.

Atwater, Harry A. 2007. “The Promise of Plasmonics.” *Scientific American* 296 (4): 56–62.

Atwater, Harry A., and Albert Polman. 2010. “Plasmonics for Improved Photovoltaic Devices.” *Nature Materials* 9 (3): 205–213.

Catchpole, K. R., and A. Polman. 2008. “Design Principles for Particle Plasmon Enhanced Solar Cells.” *Applied Physics Letters* 93 (19): 191113.

Caucheteur, Christophe, Yanina Shevchenko, Li-Yang Shao, Marc Wuilpart, and Jacques Albert. 2011. “High Resolution Interrogation of Tilted Fiber Grating SPR Sensors from Polarization Properties Measurement.” *Optics Express* 19 (2): 1656–1664.

Dai, Jin. 2012. “Design and Characterization of Plasmonic Absorbers Based on Gold Nano-Spheres.”

De Vlaminck, Iwijn, Joris Roels, Dirk Taillaert, Dries Van Thourhout, Roel Baets, Liesbet Lagae, and Gustaaf Borghs. 2007. “Detection of Nanomechanical Motion by Evanescent Light Wave Coupling.” *Applied Physics Letters* 90 (23): 233116.

Earp, Ronald Lee Jr. 1998. “Multiwavelength Surface Plasmon Resonance Sensor Designs for Chemical and Biochemical Detection,”

Economou, E. N. 1969. “Surface Plasmons in Thin Films.” *Physical Review* 182 (2): 539.

Gürel, Kemal. 2009. “Coupled Surface Plasmon Structures and Applications.” Citeseer.

Karlsson, Robert. 2004. “SPR for Molecular Interaction Analysis: A Review of Emerging Application Areas.” *Journal of Molecular Recognition* 17 (3): 151–161.

Klozenberg, J. P., B. McNamara, and P. C. Thonemann. 1965. “The Dispersion and Attenuation of Helicon Waves in a Uniform Cylindrical Plasma.” *Journal of Fluid Mechanics* 21 (03): 545–563.

Kogelnik, H., and C. V. Shank. 1972. “Coupled-Wave Theory of Distributed Feedback Lasers.” *Journal of Applied Physics* 43 (5): 2327–2335.

Kretschmann, E., and H. Raether. 1968. “Notizen: Zur Plasmaresonanzemission Im Festen Körper.” *Zeitschrift Für Naturforschung A* 23 (4): 615–617.

Maier, Stefan Alexander. 2007. “*Plasmonics: Fundamentals and Applications*.” Springer Science & Business Media.

Malitson, I. H. 1965. “Interspecimen Comparison of the Refractive Index of Fused Silica.” *JOSA* 55 (10): 1205–1209.

Müller, Joachim, Bernd Rech, Jiri Springer, and Milan Vanecek. 2004. “TCO and Light Trapping in Silicon Thin Film Solar Cells.” *Solar Energy* 77 (6): 917–930.

Otto, Andreas. 1968. “Excitation of Nonradiative Surface Plasma Waves in Silver by the Method of Frustrated Total Reflection.” *Zeitschrift Für Physik* 216 (4): 398–410.

Park, Heesoo. 2015. “Study of Surface Plasmon Resonance in Metal and Alloy Nanofilms Using Maxwell Description and Metamaterial Simulation in COMSOL.”

Raether, Heinz. 1988. “*Surface Plasmons on Smooth Surfaces*. Springer.”

Ritchie, R. H. 1973. “Surface Plasmons in Solids.” *Surface Science* 34 (1): 1–19.

Ruppin, R., and A. D. Boardman. 1982. “Electromagnetic Surface Modes.” *Wiley, Chichester 1982) Chap* 9: 345–398.

Shalabney, Atef, and Ibrahim Abdulhalim. 2012. “Prism Dispersion Effects in near-Guided-Wave Surface Plasmon Resonance Sensors.” *Annalen Der Physik* 524 (11): 680–686.

Sharma, A. K., R. Jha, and B. D. Gupta. 2007. “Fiber-Optic Sensors Based on Surface Plasmon Resonance: A Comprehensive Review.” *IEEE Sensors Journal* 7 (8): 1118–29. doi:10.1109/JSEN.2007.897946.

Spinelli, Pierpaolo, V. E. Ferry, J. Van de Groep, M. Van Lare, M. A. Verschuuren, R. E. I. Schropp, H. A. Atwater, and A. Polman. 2012. “Plasmonic Light Trapping in Thin-Film Si Solar Cells.” *Journal of Optics* 14 (2): 024002.

Stegeman, G. I., R. F. Wallis, and A. A. Maradudin. 1983. “Excitation of Surface Polaritons by End-Fire Coupling.” *Optics Letters* 8 (7): 386–388.

Ye, Yong-Hong, and Jia-Yu Zhang. 2005. “Enhanced Light Transmission through Cascaded Metal Films Perforated with Periodic Hole Arrays.” *Optics Letters* 30 (12): 1521–1523.

Yushanov, S. P., L. T. Gritter, J. S. Crompton, and K. C. Koppenhoefer. 2012. “Surface Plasmon Resonance.” In *COMSOL Conference*.

VITAE

Name Mr. Beang Sengkhun

Student ID 5710220131

Educational Attainment

Degree	Name of Institution	Year of Graduation
B. Sc. (Physics)	Burapha University, Thailand	2011

Scholarship Awards during Enrolment

The royal project for educational assistance to the Kingdom of Cambodia in Her Royal Highness Princess Maha Chakri Sirindhorn (2017).

Work – Position and Address

Teacher at Kampong Chheu Teal high school, Kampong Thom province, Cambodia.

List of Publication and Proceeding

Sengkhun, B. and Teparksorn, P. 2016. Light scattering and surface plasmon resonance on Prism-Metal-Dielectric Coupler. In: Proceeding of the 20th International Annual Symposium on Computational Science and Engineering (ANSCSE 20). 27-29 July 2016. Faculty of Science, Kasetsart University, Bangkok, Thailand.